Environmental Earth Sciences (2025) 84:245
https://doi.org/10.1007/s12665-025-12263-8

ORIGINAL ARTICLE

Spatiotemporal distribution, source identification and risk assessment of potentially toxic elements in sediments along the Alanya/Antalya coastline, Mediterranean Sea

Erhan Cengiz[1] · Murat Şirin[2] · Cafer Mert Yeşilkanat[3] · Gökhan Apaydın[4]

Received: 28 November 2024 / Accepted: 13 April 2025 / Published online: 30 April 2025

Abstract
This study investigates the concentrations of potentially toxic elements (PTEs), ecological risks, and human health effects in sediment samples from 11 points along the Alanya coastline, influenced by industrial, agricultural, and tourism activities. Energy dispersive X-ray fluorescence spectroscopy was used for analysis. The mean concentrations of Mn, Fe, Ni, Cu, Zn, Cr, and As were 281, 14, 30, 34, 66, 60, and 12 mg/kg, respectively. The enrichment factor values were ranked as follows: As (3.94), Zn (2.94), Cu (2.83), Cr (2.45), Ni (1.29), and Mn (1.19), indicating moderate enrichment for Cu, Zn, Cr, and As, and minimal enrichment for Ni and Mn. The geo-accumulation index indicated minimal contamination, supporting the conclusion that Alanya is not heavily impacted by the PTEs studied. The contamination factor values were highest for As (0.90) and lowest for Fe (0.30), indicating generally low levels of pollution. Seasonal variation was observed, with the highest degree of contamination in winter (7.09) and the lowest in autumn (5.39). The pollution load index ranged from 0.411 in autumn to 0.622 in winter, with an annual average of 0.468, indicating no pollution. The ecological risk factor values, ranging from 0.30 for Fe to 8.97 for As, did not show a significant ecological risk, with As contributing most to the risk. The potential ecological risk index averaged 15.4, which means a very low ecological risk. Additionally, the study confirmed that the overall potential human health risks remained within acceptable limits.

Keywords Potentially toxic elements · Seasonal variations · Environmental risk assessment · Source apportionment · Human health risk

Introduction

In recent decades, population growth, uncontrolled industrial expansion, rapid urbanization, and intensive agricultural practices have collectively caused significant environmental degradation (Tepe 2009; Varol and Sünbül 2018; Gopal et al. 2023; Akçay 2024; Özbay et al. 2025). Potentially toxic elements (PTEs) are a significant global concern, attracting worldwide attention due to their widespread presence in marine environments, long-term mobility, toxic properties, and detrimental impact on marine life, which in turn affects human health (Ke et al. 2017; Ustaoğlu and Tepe 2019; Liu et al. 2024; Ben-Tahar et al. 2025; Özşeker et al. 2025). The persistence of these metals in aquatic environments (rivers, lakes, groundwater, oceans) makes them a long-term environmental hazard, necessitating continuous monitoring and assessment (Gui et al. 2017; Liu et al. 2019; Gülşen-Rothmund et al. 2023; Yalçın et al. 2023; Ling et al. 2023; Atakoglu et al. 2024).

Given that the human body is unable to metabolize PTEs efficiently, these elements can become toxic when accumulated in biological tissues (Jain et al. 2008; Bai et al. 2011; Gopal et al. 2020; Özbay et al. 2025). Although essential for biological systems in trace amounts, metals such as iron (Fe), zinc (Zn), copper (Cu), and manganese (Mn) can

✉ Erhan Cengiz
erhan.cengiz@alanya.edu.tr

1 Department of Fundamental Sciences, Rafet Kayış Engineering Faculty, Alanya Alaaddin Keykubat University, 07425 Alanya, Antalya, Turkey

2 Department of Environmental Protection Technologies, Vocational School of Technical Sciences, Recep Tayyip Erdogan University, 53100 Rize, Turkey

3 Department of Mathematics and Science Education, Faculty of Education, Artvin Çoruh University, 08100 Artvin, Turkey

4 Department of Physics, Faculty of Science, Karadeniz Technical University, 61080 Trabzon, Turkey

become hazardous at elevated concentrations (Hogstrand and Haux 1991; Akçay 2024). Non-essential metals such as lead (Pb) and arsenic (As) are potent poisons that have the capacity to cause cell death, organ damage, and systemic poisoning even at low exposure levels (Damek-Poprawa and Sawicka-Kapusta 2003; Özşeker et al. 2025). Regulatory bodies such as the U.S. Food and Drug Administration (FDA) and the European Union have issued strict guidelines on the permissible levels of hazardous metals such as lead, chromium (Cr), and nickel (Ni) due to their severe health implications (Soliman et al. 2015; Ling et al. 2023; Özbay et al. 2025). Once introduced into marine environments, PTEs have the potential to bioaccumulate in aquatic organisms and enter the food chain, leading to long-term health risks for human populations (Akçay 2024).

PTE contamination in coastal and estuarine ecosystems represents a significant global environmental concern due to the toxic, persistent, and non-biodegradable nature of these substances, which have the potential to accumulate, migrate, and pose health risks (Tholkappian et al. 2018; Zhuang and Lu 2020; Odediran et al. 2021; Custodio et al. 2022; Atakoglu et al. 2024; Boukich et al. 2024; Ben-Tahar et al. 2025; Özşeker et al. 2025; Özbay et al. 2025). Recent studies in Turkish coastal environments have revealed significant PTE accumulation in marine sediments, particularly in tourism-intensive and industrialized regions such as Fethiye–Göcek Bay and the Gulf of Antalya (Yalçın et al. 2023; Atakoglu et al. 2024). These studies emphasize that the presence of metals such as Cr, Mn, Fe, Ni, Cu, Zn, and As is highly correlated with both natural geological sources and anthropogenic activities such as mining, industrial discharges, agricultural runoff, and wastewater treatment plant effluents (Akçay 2024; Özbay et al. 2025).

The Mediterranean coast of Turkey and other nations has been the subject of extensive research on PTE pollution, with multiple studies reporting varying contamination levels depending on regional industrialization, urbanization, and hydrodynamic conditions (Bastami et al. 2015; Gu et al. 2017; Bonsignore et al. 2018; Mille et al. 2018; Zaqoot et al. 2018; Nour et al. 2019; Abbasi and Mirekhtiary 2020; Öztürk et al. 2021; Yalçın et al. 2023; Atakoglu et al. 2024; Liu et al. 2024; Özbay et al. 2025). Coastal regions such as Fethiye–Göcek Bay and Manavgat have been reported to experience moderate to high contamination levels of PTEs, highlighting the need for continuous monitoring and environmental management strategies (Atakoglu et al. 2024).

Despite the growing body of research on PTE pollution in the Mediterranean, there is a noticeable lack of comprehensive studies focusing on seasonal variations in PTE contamination in certain regions. The Alanya district, which is situated in the Antalya province on Turkey's Mediterranean coast, is one such region that has not been extensively studied in terms of metal contamination. Alanya is an economically significant region, mainly supported by agriculture and tourism, both of which contribute to sources of pollution. The rapid expansion of the urban population, coupled with increasing tourism activities, places significant pressure on the coastal ecosystem. The district attracts many domestic and international visitors, contributing to significant anthropogenic pressures on the coastal environment. The tourism industry, including maritime activities, transportation, and urbanization, plays a role in the deposition of PTEs in coastal sediments (Gopal et al. 2023; Özşeker et al. 2025; Özbay et al. 2025). Additionally, agricultural activities in the region, particularly greenhouse cultivation, have been shown to introduce metal contaminants into the environment using fertilizers, pesticides, and irrigation practices (Akçay 2024; Ben-Tahar et al. 2025). These factors make Alanya's coastal region a prime candidate for PTE pollution monitoring and ecological risk assessment.

Considering these factors, the objective of the research is (1) to analyze the concentrations of specific PTEs (Cr, Mn, Fe, Ni, Cu, Zn, and As) in sediment samples from all seasons along Alanya's coast; (2) to assess pollution levels; (3) to evaluate ecological and health risks; (4) to map the spatial distribution of PTEs and health risks; and (5) to identify potential sources of pollution in the area. Understanding the dynamics of pollution in Alanya's marine environment will provide valuable data for policymakers, researchers, and environmental agencies to develop effective pollution mitigation and management strategies.

Materials and methods

Sampling, preparation, and chemical analysis of sediments

The investigation was carried out in the southern part of Turkey, off the coast of Alanya, east of Antalya. Alanya is influenced by a Mediterranean climate, with hot and dry summers and mild, rainy winters. The geological structure of the region is characterized by metamorphic rocks in the Taurus Mountains to the north, while alluvial plains are found in the south. The average annual precipitation in Alanya is approximately 950 mm (Republic of Turkey Ministry of Environment, Urbanization and Climate Change 2023). As seen in Fig. 1, sediment samples were seasonally gathered in 2022 from 11 specific locations along the Alanya coastline (Table S1). Using a stainless-steel shovel and spade, 5 kg of sediment was taken from each location, close to the mouths of rivers and streams at a depth of around 10 cm from the seabed (Böke Özkoç and Arıman 2023; Özbay et al. 2025). Two samples were taken from each location, for a total of 88 samples taken across four seasons. Table S1 of the supplemental material contains a list of the precise GPS

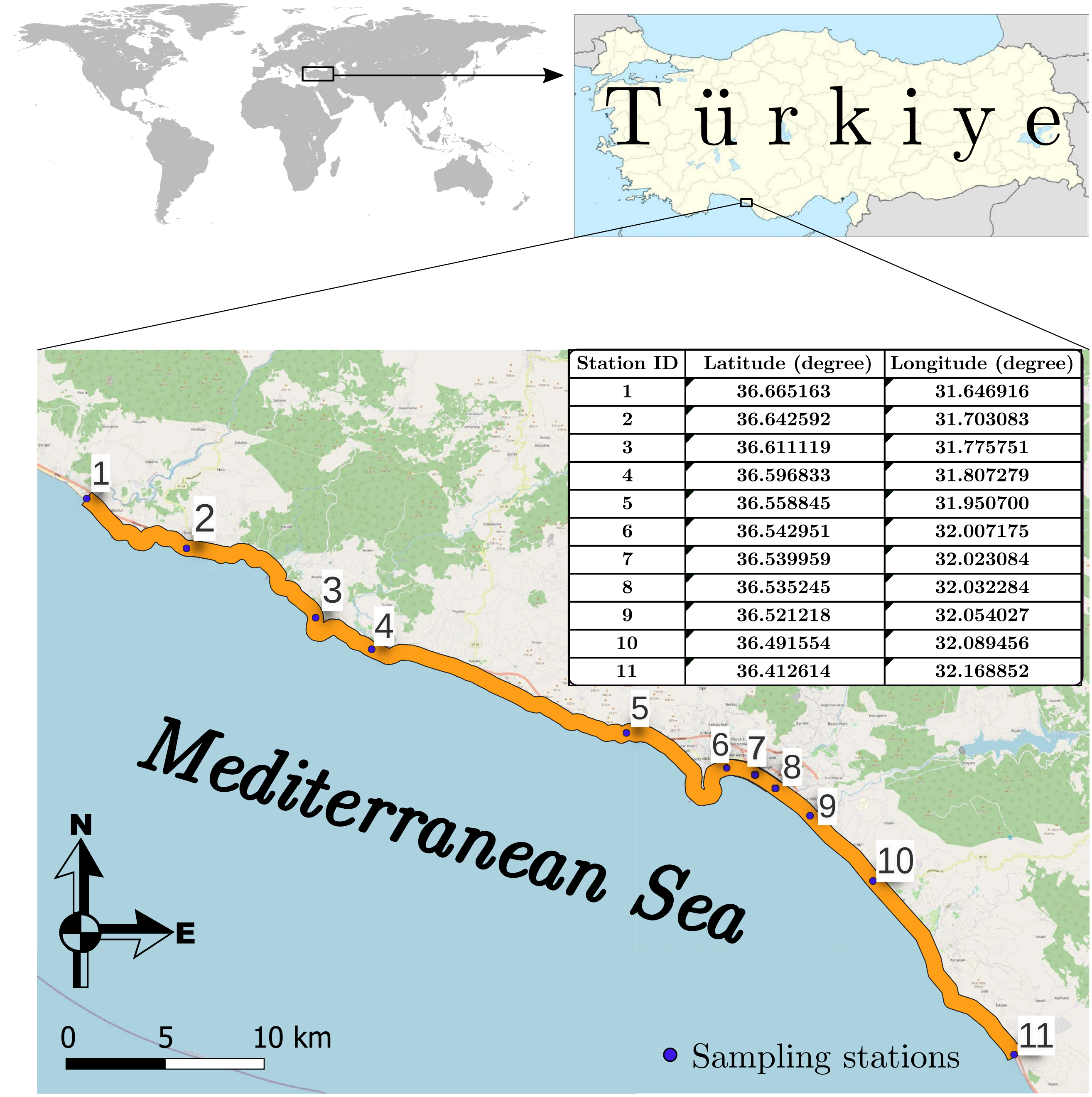

Station ID	Latitude (degree)	Longitude (degree)
1	36.665163	31.646916
2	36.642592	31.703083
3	36.611119	31.775751
4	36.596833	31.807279
5	36.558845	31.950700
6	36.542951	32.007175
7	36.539959	32.023084
8	36.535245	32.032284
9	36.521218	32.054027
10	36.491554	32.089456
11	36.412614	32.168852

Fig. 1 The study area and the locations of the stations

coordinates of the sampling locations. Sediment samples were carefully transferred into plastic bags. From each station 500 g of samples were placed in glass containers and left to dry in the laboratory environment where air conditioning and cleanliness were controlled. Subsequently, all samples were dried in an oven at 105 °C for 24 h to obtain a constant weight (Wang et al. 2021; Aydın et al. 2023; Ling et al. 2023). After drying, samples were ground in an agate mortar and sieved using a 63-micron sieve (Ravisankar et al. 2015; Kumar et al. 2017; Ni et al. 2018; Kırıs and Baltas 2021; Akçay 2024). Prior to metal analysis, the processed samples were stored in plastic containers, which were cleaned with a HCl–HNO_3 (1:1 v/v) mixture, and placed in a desiccator (Baltas et al. 2020; Apaydın et al. 2022; Akçay 2024).

For Energy dispersive X-ray fluorescence spectroscopy (EDXRF) measurements, the induction fusion fluxer device (Equilab F2, Madrid, Spain), available at the RTEU Central Research Laboratory Application and Research Center was used to prepare glassy sediment sample tablets.

This method helps minimize the influence of matrix effects, roughness, and particle size variability. To prepare the tablets, X-ray flux (XRF Scientific, Osborne Park WA 6017, Australia), a mixture of lithium tetraborate 66% ($Li_2B_4O_7$) and lithium metaborate (34% $LiBO_2$), was added to the sediment samples. The weight ratio of the sample to the fusion material in the glass tablet was maintained at 1:10 (w/w). For creating glass tablets with a diameter of 40 mm, 1 g of sediment and 10 g of lithium tetraborate/lithium metaborate mixture were precisely weighed using an analytical balance. The mixture was then transferred into a mortar and mixed for 10 min. Subsequently, the resulting blend, obtained using the melter, was poured into crucibles with an internal volume of 25 mL, consisting of 5% gold and 95% platinum. The melting process was executed at 1150 °C for 8 min, using the method specifically designed within the device for sediment. The 40-mm diameter platinum molds were automatically filled with the molten liquid sample, which was then left to cool at room temperature. The glass tablets obtained were labeled according to the respective sampling stations and stored in a vacuum desiccator until EDXRF measurements were performed (Bell et al. 2020; Balaram and Subramanyam 2022).

The concentrations of Cr, Mn, Fe, Ni, Cu, Zn, and As in sediment samples were measured using a Rigaku NEX–CG EDXRF Spectrometer. Each sample was evaluated in triplicate for one hour using a 50 W palladium X-ray tube and a Silicon Drift Detector (SDD) with a resolution of 150 eV. To ensure accuracy, the library was calibrated weekly with pure elements, and the Multichannel Analyzer (MCA) was calibrated daily prior to analysis. Certified standards for Cu, Sn, and SiO_2 were employed as calibration references (Croffie et al. 2020; Odabas et al. 2021; Yalçın et al. 2023). Additionally, the Multichannel Analyzer (MCA) was calibrated daily before starting any analysis.

The limit of detection (LOD) for EDXRF was calculated using the method described by Kadachi and Al-Eshaikh (2012):

$$LOD = \frac{3}{s}\sqrt{\frac{I_b}{T}} \tag{1}$$

LOD's for the metals examined were determined, which were based on sensitivity in counts per mg/kg (s), background intensity (I_b), and count time in seconds (T): 0.02 mg/kg Cr, 0.08 mg/kg Fe, 0.09 mg/kg Mn, 0.10 mg/kg Ni, 0.08 mg/kg Cu, 0.05 mg/kg Zn, and 0.04 mg/kg As. Calibration and quality assessment were performed using the certified reference material, estuary sediment (NW–WQB–1), with an average recovery of 101.9% for all investigated metals, which falls within the permitted range of 80% to 110% (Table S2). These results confirm that the recovery percentage meets the standard criteria (Anandkumar et al. 2017, 2018; Baltas et al. 2020; Hossain et al. 2022; Akçay 2024).

Assessment of potentially toxic elements pollution

In this study, indices such as enrichment factor *(EF)*, geo-accumulation index (I_{geo}), contamination factor (C_f), modified degree of contamination (mC_d), pollution load indices (*PLI* and PLI_{zone}), ecological risk factor (E_r), and potential ecological risk factor (*PERI*) were utilized to assess the environmental concerns associated with PTE contamination in sediments (Gope et al. 2017; Jayarathne et al. 2018; Gopal et al. 2021, 2023). These indices use Krauskopf (1985) values as a benchmark to offer a quantitative evaluation of pollution levels (Krauskopf 1985; Chandrasekaran and Ravisankar 2015; Baltas et al. 2020; Akçay 2024). Table S3 provides comprehensive formulas and classifications for every index.

Human health risk assessment

The human health risk assessment was conducted in two parts, addressing non-carcinogenic and carcinogenic risks, based on the specific exposure pathways of toxic heavy metals. Furthermore, the model suggested by the US Environmental Protection Agency (USEPA 1989, 1993, 1996, 2002, 2010) was used for these assessments.

Exposure assessment

The main exposure pathways to PTEs in sediment samples in this study were identified as direct ingestion and dermal absorption (Böke Özkoç and Arıman 2023). Equations (2) and (3) were used to determine the average daily dose (*ADD*), expressed in mg kg^{-1} day^{-1}, of hazardous PTEs impacting humans via these pathways.

$$ADD_{ing} = \frac{C \times EF \times ED \times CF \times IR_{ing}}{AT \times BW} \tag{2}$$

$$ADD_{derm} = \frac{C \times EF \times ED \times SA \times AF \times CF \times ABS}{AT \times BW} \tag{3}$$

Table S4 lists the definitions and reference values for all parameters in the equations (Ferreira-Baptista and De Miguel 2005; Li et al. 2017; Jayarathne et al. 2018; Cui et al. 2020; Abdelaal et al. 2024; Ben-tahar et al. 2025; Özşeker et al. 2025).

Non-carcinogenic risk assessment

Key metrics for evaluating possible non-cancer effects from PTE exposure are the Hazard Index (*HI*) and Hazard Quotient (*HQ*) (Wei and Yang 2010; Jayarathne et al. 2018; Wu et al. 2020; Yesilkanat and Kobya 2021). For each exposure pathway, *HQ* is the ratio of a metal's daily intake to its reference dose (*RfD*, in mg kg^{-1} day^{-1}), and *HI* is the sum of all *HQs* (USEPA 1989). For adults, Eqs. (4) and (5) are used to compute *HQ* and *HI* independently:

$$(HQ)_n = \underbrace{\left(\frac{ADD_{ing}}{RfD_{ing}}\right)_n}_{(HQ-ingestion)_n} + \underbrace{\left(\frac{ADD_{derm}}{RfD_{derm}}\right)_n}_{(HQ-dermal)_n} \tag{4}$$

$$HI = \sum_{n=1}^{N} (HQ)_n \tag{5}$$

n denotes the number of PTEs examined in this study, with $(RfD_{ing})_n$ and $(RfD_{derm})_n$ denoting the reference doses for oral intake and dermal contact for the nth metal. Table S5 provides the reference dose estimates for each element, obtained from previous research (Ferreira-Baptista and De Miguel 2005; Wei et al. 2015; Kamunda et al. 2016; Adimalla 2020; Özbay et al. 2025). The USEPA (1989) defines a Hazard Index (*HI*) value of less than 1 as indicating either minimal or no non-carcinogenic health impacts, whereas $HI > 1$ indicates potential concerns for non-carcinogenic.

Carcinogenic risk assessment

Carcinogenic risk (*CR*), as defined by Eq. (6) for adults, is the probability of acquiring cancer because of prolonged exposure to carcinogenic metals, considering the exposure routes and average daily doses (*ADD*) of metals such as chromium (Cr), nickel (Ni), and arsenic (As) (USEPA 1989; Shabbaj et al. 2018).

$$CR_i = \left(ADD_{ing} \times SF_{ing}\right)_i + \left(ADD_{derm} \times SF_{derm}\right)_i \tag{6}$$

In this study, the target metal is represented by (*i*), with $(SF_{ing})_i$ and $(SF_{derm})_i$ denoting the carcinogenic slope factors for ingestion and dermal contact, respectively. Table S5 shows the slope factor values for the carcinogenic metals examined (Ferreira-Baptista and De Miguel 2005a; Wei and Yang 2010; Kamunda et al. 2016b; Adimalla 2020; Yesilkanat and Kobya 2021; Özbay et al. 2025). The cancer risk (CR_i) is categorized as extremely low ($CR_i \le 10^{-6}$), low ($10^{-6} < CR_i \le 10^{-4}$), moderate ($10^{-4} < CR_i \le 10^{-3}$), high ($10^{-3} < CR_i \le 0.1$), and very high ($CR_i \ge 0.1$) (Ge et al. 2013). The total cancer risk (*TCR*) is the sum of individual cancer risks for all carcinogenic metals and is classified in the same way as CR_i (Wei et al. 2009; Li and Jia 2018; Zhao et al. 2019; Baltas et al. 2020; Yesilkanat and Kobya 2021; Özbay et al. 2025).

$$TCR = \sum_{i=1}^{n} (CR)_i \tag{7}$$

Statistical and geostatistical analyses and software resources

Descriptive and inferential statistical analyses were employed to investigate metal concentrations in the sediment samples. Basic descriptive statistics-including minimum, maximum, mean, and standard deviation—were calculated for each metal. To further evaluate the distribution characteristics and variability of metal concentrations, additional metrics such as the coefficient of variation (CV), skewness, and kurtosis were computed on an annual basis.

The coefficient of variation (CV) served as a key indicator of variability and potential anthropogenic influence. High CV values were interpreted as evidence of greater anthropogenic input, whereas low values suggested dominance by natural geochemical processes (Cai et al. 2015; Marcinkonis et al. 2011).

Data normality was initially assessed using the Kolmogorov–Smirnov test ($p > 0.05$) and further evaluated through skewness and kurtosis values. Skewness measures the asymmetry of the distribution: values close to zero indicate symmetry, while positive and negative values suggest right- and left-skewed distributions, respectively. In environmental sediment studies, positive skewness is often interpreted as the result of sporadic or localized anthropogenic contamination, which causes infrequent but extremely high concentrations (El Nemr and El-Said 2017; Khalil et al. 2016). Kurtosis assesses the peakedness and tail weight of the distribution. A positive kurtosis indicates a sharp, heavy-tailed distribution, which may reflect occasional inputs of high-concentration pollutants, while a negative kurtosis reflects a flatter, more evenly spread distribution typical of natural geogenic sources (Field et al. 2012; El-Said et al. 2014; El Nemr and El-Said 2017). These parameters help validate the assumption of normality, strengthening the reliability of subsequent analyses (Lu et al. 2010; Kelepertzis 2014; Chandrasekaran and Ravisankar 2015).

Levene's test was used to examine the homogeneity of variances. To explore potential sources and interrelationships of potentially toxic elements (PTEs), multivariate statistical techniques were applied, including Pearson correlation coefficient (PCC), principal component analysis (PCA), and hierarchical cluster analysis (HCA). All statistical tests were conducted at a 95% confidence level ($p < 0.05$) using SPSS 29 and the R statistical environment (R Core Team 2024). Graphical representations of the results were created

Table 1 Summary statistics of annual heavy metal concentrations in sediments (n = 88)

Elements	Min (mg/kg)	Max (mg/kg)	Mean (mg/kg)	SD[a] (mg/kg)	K–S test	Skewness	Kurtosis	CV[b] (%)	BGV[c]	*TEL*[d]	*PEL*[d]
Mn	83.64	739.61	281.00	141.96	0.68	− 0.234	− 0.341	50.52	850	–	–
Fe	3818.86	41,685.76	14,275.47	8,384.17	0.56	0.021	− 0.580	58.73	47,000	–	–
Ni	8.64	78.58	30.06	18.54	0.62	0.282	− 0.843	61.69	80	15.9	42.8
Cu	22.37	51.93	34.39	7.07	0.77	0.028	− 0.672	20.56	50	18.7	108
Zn	38.56	98.82	66.23	16.93	0.56	− 0.080	− 0.842	25.56	90	124.0	271
Cr	10.95	217.58	59.96	13.25	1.20	0.610	− 0.799	103.18	100	52.3	160
As	5.00	32.00	11.66	6.30	2.04	0.885	− 1.025	54.00	20	7.24	41.60

n sampling number

[a]Standard deviation (SD)

[b]Coefficent of variation(CV) (%)

[c]Background value (BGV) of chemical elements in the shale (Krauskopf 1985)

[d]*TEL* threshold effect level, *PEL* probable effect level. Sediment quality guidelines (SQG) (Long et al. 1995)

using OriginPro 2024b (Tian et al. 2017; Cai et al. 2019; Baltas et al. 2020). The results, summarized in Table 1, provide meaningful insights into the spatial distribution, variability, and possible geochemical origins of metals in the sediment samples.

Spatial and geostatistical modeling was also performed using the R environment, incorporating the widely used gstat (Pebesma 2004) and sp (Pebesma and Bivand 2005) packages for spatial data analysis in environmental studies. Map visualizations were generated using Quantum Geographic Information System (QGIS) version 3.34.3. All interpolation maps were produced with a grid resolution of 100 × 100 m (equivalent to 1 hectare). These tools are widely employed in environmental monitoring research (Baltas et al. 2019; Yesilkanat and Kobya 2021).

Results and discussion

Potentially toxic element concentrations

Table 1 summarizes descriptive statistics for the annual metal concentrations determined in sediment samples and compares them with the average shale values supplied by Krauskopf (1985). The analysis showed that the metal concentrations in the sediments varied greatly, with ranges from 83.64 to 739.61 mg/kg for Mn, 3818.86 to 41,685.76 mg/kg for Fe, 8.64 to 78.58 mg/kg for Ni, 22.37 to 51.93 mg/kg for Cu, 38.56 to 98.82 mg/kg for Zn, 10.95 to 217.58 mg/kg for Cr, and 5.00 to 32.00 mg/kg for As. The average values for Mn, Fe, Ni, Cu, Zn, Cr, and As were determined to be 281.00 ± 141.96 mg/kg, 14,275.47 ± 8314.17 mg/kg, 30.06 ± 18.54 mg/kg, 34.39 ± 7.07 mg/kg, 66.23 ± 16.93 mg/kg, 59.96 ± 13.25 mg/kg, and 11.66 ± 6.30 mg/kg, respectively. The most common of these metals was Fe, which was followed in decreasing order by Mn, Zn, Cr, Cu, Ni, and As. The presence of Fe and Mn at the highest levels in coastal sediments is a common phenomenon, which is also supported by these studies (Gopal et al. 2020; Kodat and Tepe 2023). However, the ranking of elements such as Zn, Cr, Cu, Ni, and As varies depending on regional geochemical processes, anthropogenic influences, and industrial activities. The average concentrations of each metal examined were notably lower than the average shale values that Krauskopf (1985) reported.

High SD values in sediment PTE distribution stem from spatial heterogeneity, seasonal changes, and anthropogenic impacts. Hydrodynamic processes, grain size variations, and pollution sources contribute to these fluctuations (Şener et al. 2023; Duman et al. 2025; Özşeker et al. 2025). Findings confirm that both natural and human factors drive these variations, emphasizing the need for continuous monitoring of sediment transport and metal pollution. The Kolmogorov–Smirnov (K–S) test was used to determine if the data fit a normal distribution. When the p value is greater than 0.05, the test indicates that the data are normally distributed (Kelepertzis 2014; Cai et al. 2015; Baltas et al. 2020). Figure 2 shows that all metal concentrations followed a normal distribution, according to the K–S test results. To verify normality, skewness values were also investigated. A normal distribution is suggested by a skewness value between − 1 and 1, but values outside of this range show deviations from normality (Chandrasekaran and Ravisankar 2015; Baltas et al. 2020). The analysis of the metals examined in this study confirmed the normal distribution of the data, as indicated by skewness and kurtosis values within the permissible range (Lu et al. 2010; Cai et al. 2019). Similar results were reported in studies conducted along the Egyptian Mediterranean coast, where skewness values ranged between − 0.66 and + 0.45, supporting the symmetric nature

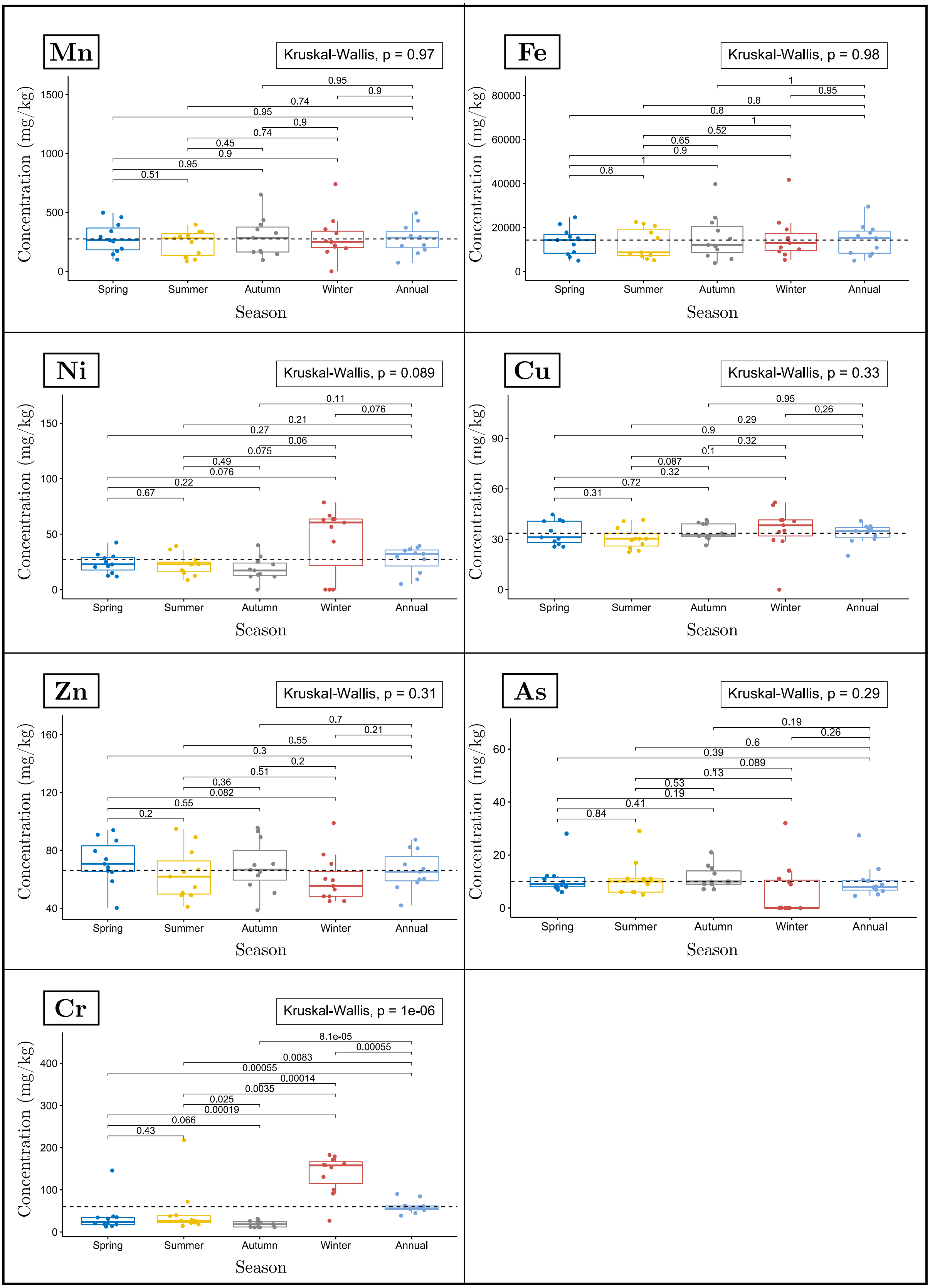

Fig. 2 Box-and-whisker diagram of potentially toxic element levels according to seasons and Kruskal–Wallis test results

of metal distributions in many sampling stations (El-Said et al. 2014; El Nemr and El-Said 2017). Negative skewness values were associated with areas undergoing erosion and sediment coarsening, while positive values reflected depositional environments rich in carbonates. Kurtosis values in these studies also ranged widely, from very platykurtic (0.48) to very leptokurtic (2.82), indicating variability in sediment sorting and transport dynamics. For example, sediments with well-sorted carbonate-rich fractions showed high kurtosis, whereas mixed sediments in dynamic zones had flatter distributions (Khalil et al. 2016). Studies in Çandarlı Gulf, Türkiye have shown that higher skewness values in winter are linked to increased stormwater runoff, bringing in high loads of metals from agricultural and urban sources (Duman et al. 2025). Additionally, in marine environments with dynamic hydrodynamics, kurtosis fluctuations indicate the reworking and redeposition of sediments, particularly in low-energy environments, where fine particles and associated metals accumulate over time (Şener et al. 2023). These findings highlight the importance of seasonal monitoring to assess the variability of metal contamination and its transport dynamics in coastal environments.

To evaluate metal concentration variability, the coefficient of variation (CV) was used. Higher CV values indicate anthropogenic sources, while lower CV values suggest natural origins (Marcinkonis et al. 2011; Cai et al. 2015; Mamut et al. 2017; Baltas et al. 2020). The CV values for Mn (50.52%), Fe (58.73%), Ni (61.69%), Cu (20.56%), Zn (25.56%), Cr (103.18%), and As (54.00%) are displayed in Table 1. According to CV classifications, Mn, Fe, Ni, Zn, and As exhibited moderate variability ($25\% < CV < 75\%$), while Cr showed considerable variability ($CV > 75\%$), indicating a strong anthropogenic influence. In contrast, Cu displayed minimal fluctuation ($CV < 25\%$), suggesting a predominantly natural origin, likely from the parent material of the sediment and topography (Mamut et al. 2017). These findings are consistent with studies from the Southeast Indian coast, where Cr exhibited high variability due to industrial discharges and urban runoff (Gopal et al. 2021). Topography plays a key role in the distribution of PTEs in sediments. It influences runoff, drainage, and erosion, which shape sediment metal concentrations (Du Laing et al. 2009; Liu et al. 2016). Marine transport and coastal erosion are major contributors to metal accumulation, as observed in studies of the Yellow River in China and Indian coastal regions (Zhang et al. 2018; Gopal et al. 2023).

A comparison with Sediment Quality Guidelines (SQGs) was conducted to assess potential ecological risks. The mean concentrations of Cr, As, Cu, and Ni exceeded the Threshold Effect Level (*TEL*), indicating potential ecological risks. However, Zn levels were below *TEL*, suggesting a low probability of adverse effects (Table 1). These results align with studies on Turkish and North African coastal sediments, in which Cr and As have been identified as primary pollutants (Ben-Tahar et al. 2025).

Despite elevated *TEL* values for some metals, their concentration remained below the Probable Effect Level *(PEL),* meaning that adverse effects are unlikely under normal conditions. This finding is consistent with reports from the Indian Ocean and Eastern Mediterranean, where Cu and Zn levels were found to be below the *PEL* but still required monitoring (Gopal et al. 2021).

The average concentrations of PTEs (Mn, Fe, Ni, Cu, Zn, Cr, and As) found in this study were compared with previous research, as presented in Table S6. The Mn concentration (281 mg/kg) observed in Alanya was lower than that recorded in some Turkish coastal regions, such as the Eastern Mediterranean coast (671.02 mg/kg; Yalçın et al. 2023) and the Middle and Eastern Black Sea Coast (565.38 mg/kg; Apaydın et al. 2022), but higher than levels reported in the Red Sea (198.76 mg/kg; Nour et al. 2019) and Saudi Arabian coastal sediments (184 mg/kg; El-Sorogy et al. 2020). The Fe concentration (14,275.47 mg/kg) in Alanya was significantly lower than the values recorded in the Middle and Eastern Black Sea Coast (46,000 mg/kg; Apaydın et al. 2022) but higher than those measured in the Egyptian Mediterranean (13,256 mg/kg; Soliman et al. 2015) and the Red Sea (8451.62 mg/kg; Nour et al. 2019). The increase in Fe and Mn concentrations is primarily linked to sediment composition, redox-driven mobilization, and seasonal hydrodynamic changes. These elements accumulate in fine-grained sediments, binding with organic matter and clay minerals, which enhances their retention (Duman et al. 2025). Additionally, oxygen fluctuations in sediment layers promote Fe and Mn cycling, leading to seasonal variations in their distribution (Şener et al. 2023). Studies have also shown that Mn is strongly influenced by salinity gradients and oxygen availability, whereas Fe tends to accumulate in organic-rich sediments (Atakoglu et al. 2024). These findings confirm that natural geochemical processes and sediment properties play a dominant role in Fe and Mn enrichment in the study area.The Ni levels (30.06 mg/kg) were higher than those reported in studies from the Caspian Sea (16.6 mg/kg; Gholizadeh and Patimar 2018) and the Red Sea (17.52 mg/kg; Nour et al. 2019), yet lower than those from Turkey (108.59 mg/kg; Yalçın et al. 2023; 34.38 mg/kg; Apaydın et al. 2022). The higher Ni concentration in the study area is mainly attributed to agricultural runoff, wastewater discharges from tourism activities, and atmospheric deposition. Similar studies in Fethiye Bay and Giresun, Türkiye, identified fertilizer use, pesticide residues, and untreated wastewater as key contributors to Ni pollution (Apaydın et al. 2022; Yalçın et al. 2023). Additionally, insufficient wastewater treatment in high-tourism areas leads to direct discharge into coastal waters, increasing heavy metal accumulation in sediments (Atakoglu et al. 2024). Similarly, Cu levels (34.39 mg/kg) were above values reported in other regions but significantly lower than values recorded in Turkish coastal sediments, particularly in the Eastern Black Sea Coast (3107.3 mg/kg; Alkan et al. 2020) and the Middle and Eastern Black Sea Coast (104.06 mg/kg; Apaydın et al. 2022). Zn levels (66.23 mg/kg) followed a similar trend, lower than those reported in Turkey (4259.5 mg/kg; Alkan et al. 2020; 109.88 mg/kg; Apaydın et al. 2022) but exceeding values from regions such as the Egyptian Mediterranean coast (22.19 mg/kg; Soliman et al. 2015) and the Red Sea (44.15 mg/kg; Nour et al. 2019). Cr concentrations (59.56 mg/kg) in Alanya were higher than those from the Eastern Black Sea Coast (40.2 mg/kg; Alkan et al. 2020) and Caspian Sea (17.9 mg/kg; Gholizadeh and Patimar 2018) but lower than those observed in Egypt (82.74 mg/kg; Soliman et al. 2015) and the Antalya Gulf (891.88 mg/kg; Yalçın et al. 2023). The higher Cr concentration in the study area is primarily linked to agricultural activities, industrial inputs, and untreated wastewater discharges. Similar findings in Türkiye and Egypt have shown that Cr contamination is often associated with pesticide residues, fertilizer runoff, and urban wastewater effluents (Yalçın et al. 2023; Apaydın et al. 2022; Soliman et al. 2015). Additionally, in tourism-heavy coastal areas, untreated sewage contributes to elevated Cr levels, as observed in Mediterranean and Red Sea coastal regions (Atakoglu et al. 2024; Nour et al. 2022). Lastly, the As levels (11.66 mg/kg) were lower than those measured in Turkish coastal regions such as the Eastern Black Sea Coast (208.2 mg/kg; Alkan et al. 2020) but exceeded values reported in the Caspian Sea (7.4 mg/kg; Gholizadeh and Patimar 2018) and the Red Sea (6.6 mg/kg; (El-Sorogy et al. 2020)). These findings highlight regional differences in PTE contamination and emphasize the necessity for continued monitoring and environmental protection measures in coastal ecosystems.

Figure 2 shows the seasonal variance in PTE levels using a box-whisker plot. The Kruskal–Wallis test found no significant seasonal changes in metal concentrations, except for Cr ($p < 0.05$). The Mann–Whitney pairwise comparison revealed that, other than Cr, there were no significant variations in mean concentrations among seasons. There were significant changes in chromium (Cr) concentrations across autumn, winter, spring, and summer ($p < 0.05$), with winter having the highest concentration. These results are consistent with the study conducted in the southeastern Black Sea region of Turkey, where Cr contamination peaked during the winter and spring seasons due to stormwater runoff (Kodat and Tepe 2023).

Pollution assessment

Enrichment factor (*EF*) and geo-accumulation index (I_{geo})

Figure 3 illustrates the seasonal variation in the enrichment factor (*EF*) and geo-accumulation index (I_{geo}) values, as well as the average contribution from each metal during such variations. A summary of the *EF* and I_{geo} values calculated for the sediments is presented in Table 2. As shown in Fig. 3, the highest *EF* values were recorded during winter, with chromium (Cr) contributing the most (an average of 5.32). According to Edokpayi et al. (2017), metal enrichment in aquatic environments decreases in winter due to higher water volume, whereas it increases in summer due to evaporation effects. Similarly, Islam et al. (2015) noted that metal concentrations tend to be lower in the rainy season due to dilution, although specific activities and local pollution sources can cause exceptions to this trend. In line with these studies, this research also found higher enrichment in winter compared to summer months (Zhao et al. 2014; Rajeshkumar et al. 2018). The reason for the increase in metal concentration in sediments during winter is due to increased precipitation. As a result, water from surrounding areas carries pesticides, agricultural fertilizers, and PTEs into the aquatic environment, and the PTEs that mix with the water settle and accumulate in the sediments. The reduction in biological activity at low temperatures limits the biological retention of PTEs, leading to increased accumulation (Sancer and Tekin-Özan 2016).Throughout the other months and in the annual analysis, arsenic (As) was the primary contributor. The average *EF* values of the PTEs were ranked as follows: Cr (4.56) > As (3.94) > Zn (2.94) > Cu (2.83) > Ni (1.29) > Mn (1.19) (Table 2). According to Table S3, As, Zn, Cu, and Cr show moderate enrichment, while Ni and Mn exhibit minimal enrichment. The moderate enrichment levels of As, Cu, Zn, and Cr in the study area are primarily caused by agricultural runoff, industrial discharges, and untreated wastewater from tourism-related activities. Research in Turkish coastal areas has shown that As, Cu and Zn accumulation is linked to fertilizer use, pesticide applications, and sewage effluents, while Cr pollution originates from industrial waste and urban runoff (Yalçın et al. 2023; Apaydın et al. 2022). Similar contamination patterns were observed in Çandarlı Gulf, where industrial proximity increased *EF* values for metals (Duman et al. 2025). Additionally, findings from the Pearl River Delta indicate that chromium (Cr) and arsenic (As) pollutions are strongly associated with agricultural pesticide applications (Liang et al. 2025). These results emphasize the need for enhanced wastewater treatment and sustainable agricultural practices to reduce PTE accumulation in sediments. In general, when the *EF* value is around 1, it is thought that metal enrichment results from crustal materials or natural wear processes. If the *EF* value is greater than 1.5, the main source of such enrichment is anthropogenic inputs (Tholkappian et al. 2018). In this study, the *EF* values for Mn and Ni were below 1.5, indicating that their sources were predominantly natural (crustal materials and erosion processes). In contrast, *EF* values above 1.5

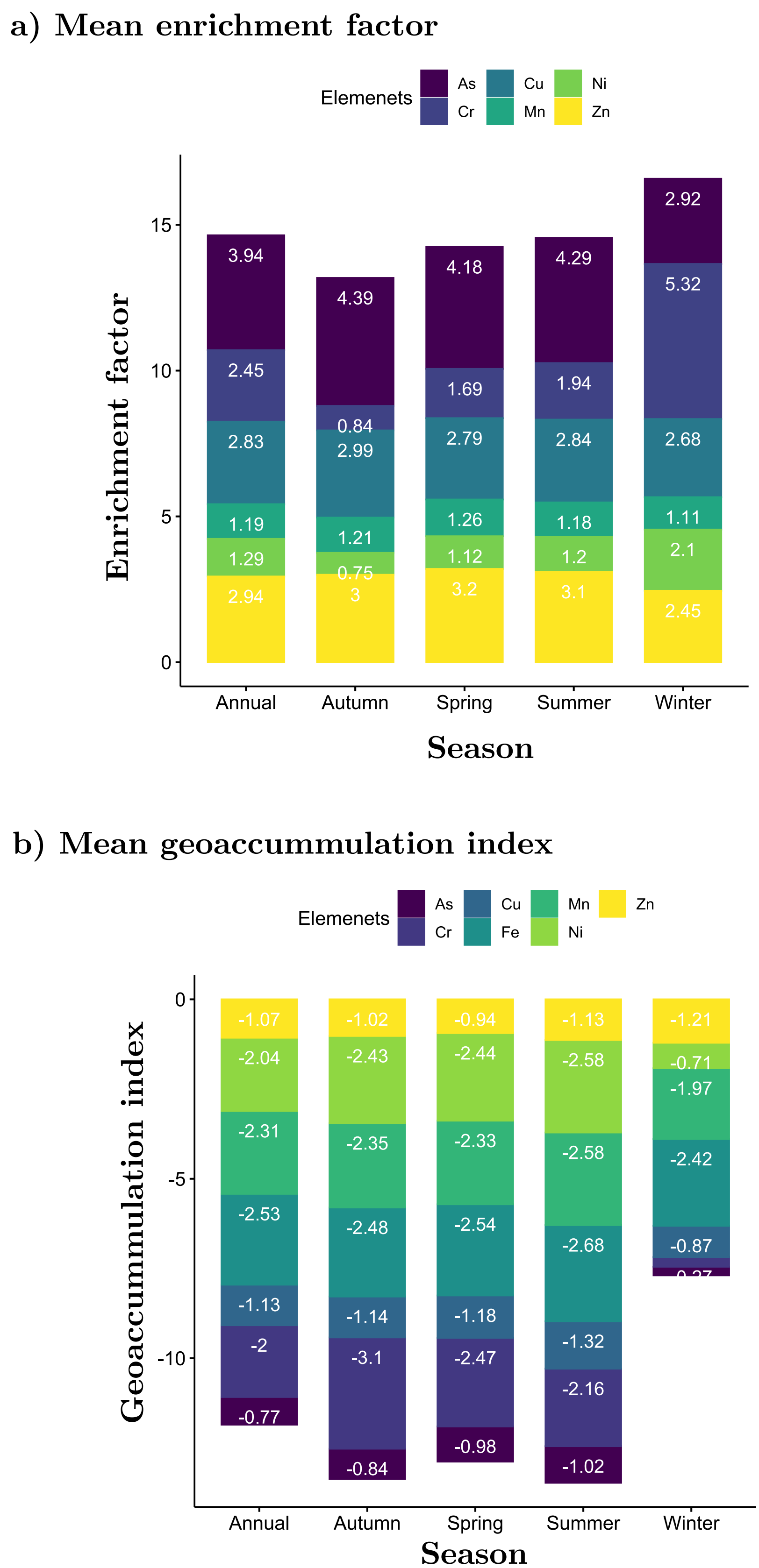

Fig. 3 Seasonal distribution of enrichment factor (EF) and geoaccumulation index (Igeo) values and average contributions of elements

Table 2 Descriptive statistics of pollution and ecological risk indices

Ecological risk index	*EF*			I_{geo}			C_f			E_r		
Elements	Mean	Min	Max	Mean	Min	Max	Mean	Min	Max	Mean	Min	Max
Mn	1.19	0.53	2.61	−2.31	−3.93	−0.79	0.33	0.10	0.87	0.33	0.10	0.87
Fe	–	–	–	−2.53	−4.21	−0.76	0.30	0.08	0.89	0.30	0.08	0.89
Ni	1.29	0.40	5.10	−2.04	−3.80	−0.61	0.38	0.11	0.98	1.88	0.54	4.91
Cu	2.83	0.86	6.49	−1.13	−1.75	−0.53	0.69	0.45	1.04	3.44	2.24	5.19
Zn	2.94	1.23	5.60	−1.07	−0.45	−1.07	0.74	0.43	1.10	0.74	0.43	1.10
Cr	4.56	0.23	11.16	−2.00	−3.78	0.54	0.60	0.11	2.18	1.20	0.22	4.35
As	3.94	1.37	21.91	−0.77	−1.96	0.71	0.90	0.38	2.46	8.97	3.85	24.62

Ecological risk index	Mean	Min	Max
PLI	0.73	0.00	1.21
C_d	3.49	2.12	5.80
mC_d	5.89	5.39	7.09
PERI	15.07	8.33	29.41

for Cr, Cu, Zn, and As suggest significant anthropogenic contributions from industrial, agricultural, and tourism-related activities (Öztürk et al. 2021; Gopal et al. 2021).

In relation to the geoaccumulation index (I_{geo}), Fig. 3b illustrates that the average I_{geo} values for all metals were negative ($I_{geo} < 0$), signifying no significant pollution throughout the seasons. Notably, Fe was the largest contributor to the I_{geo} values in all seasons except autumn. Table 2 shows the ranking of I_{geo} values: As (−0.77) > Zn (−1.07) > Cu (−1.13) > Cr (−2.00) > Ni (−2.04) > Mn (−2.31) > Fe (−2.53). According to the Müller classification in Table S3, these findings confirm that the Alanya region is not significantly polluted by PTEs (Baltas et al. 2020).

Contamination factor (C_f), modified degree of contamination (*mCd*), and pollution load index (*PLI*)

Table 2 presents the C_f and *PLI* values for metals. The C_f values decreased in the following order: As (0.90), Zn (0.74), Cu (0.69), Cr (0.60), Ni (0.38), Mn (0.33), and Fe (0.30). Based on the average C_f values, minimal pollution was observed in the investigated region for all metals, as shown in Table S3. Figure 4a illustrates the seasonal contribution of each element to the degree of contamination, expressed as percentages. Arsenic (As) contributes the most thorougt the year, in all seasons except winter, where chromium (Cr) takes the highest contribution. The lowest contribution comes from Fe in all seasons except autumn, where Ni has the lowest contribution Fig. 4b presents the seasonal cumulative mC_d levels, which serve as an indicator of sediment C_f. The highest mC_d level (7.09) was observed in winter, the lowest (5.39) in autumn, with the annual average at 5.89. According to the mC_d contamination grading in Table S3, the study area exhibits a high level of contamination. Figure 4c illustrates the seasonal variation in the distribution of the Pollution Load Index (*PLI*) levels, another indicator of PTE pollution. The highest average *PLI* value was recorded in winter (0.622), while the lowest was in autumn (0.411). The annual average *PLI* (0.468) suggests that the study area is not polluted ($PLI < 1$) (Öztürk et al. 2021) (Table S3). In addition, the Kruskal–Wallis test indicated that seasonal variations in *PLI* were statistically significant ($p < 0.05$). The Mann–Whitney pairwise comparisons test revealed that winter was the primary season responsible for these observed differences. The higher *PLI* value in winter detected in the study area is primarily due to increased runoff, reduced dilution capacity and hydrodynamic changes associated with seasonal weather patterns. Studies indicate that heavy precipitation and storm events during winter lead to greater transport of PTEs from agricultural fields, urban runoff, and atmospheric deposition into coastal sediments (Vinothkannan et al. 2022). Similar seasonal trends were observed in Çandarlı Gulf, Türkiye, where rainfall-driven runoff significantly increased the pollution load index (*PLI*) and sediment contamination levels (Duman et al. 2025). Additionally, research on Beyşehir Lake found that lake water circulation and sedimentation rates were lower in winter, leading to the accumulation of contaminants (Şener et al. 2023; Ben-tahar et al. 2025). These factors explain the seasonal variation in pollution levels, emphasizing the need for continuous monitoring and improved watershed management in coastal areas.

Potential ecological risk index (*PERI*) and ecological risk factor (E_r)

Table 2 presents the ecological risk factor (*Er*) and potential ecological risk index (*PERI*) values for the PTEs studied.

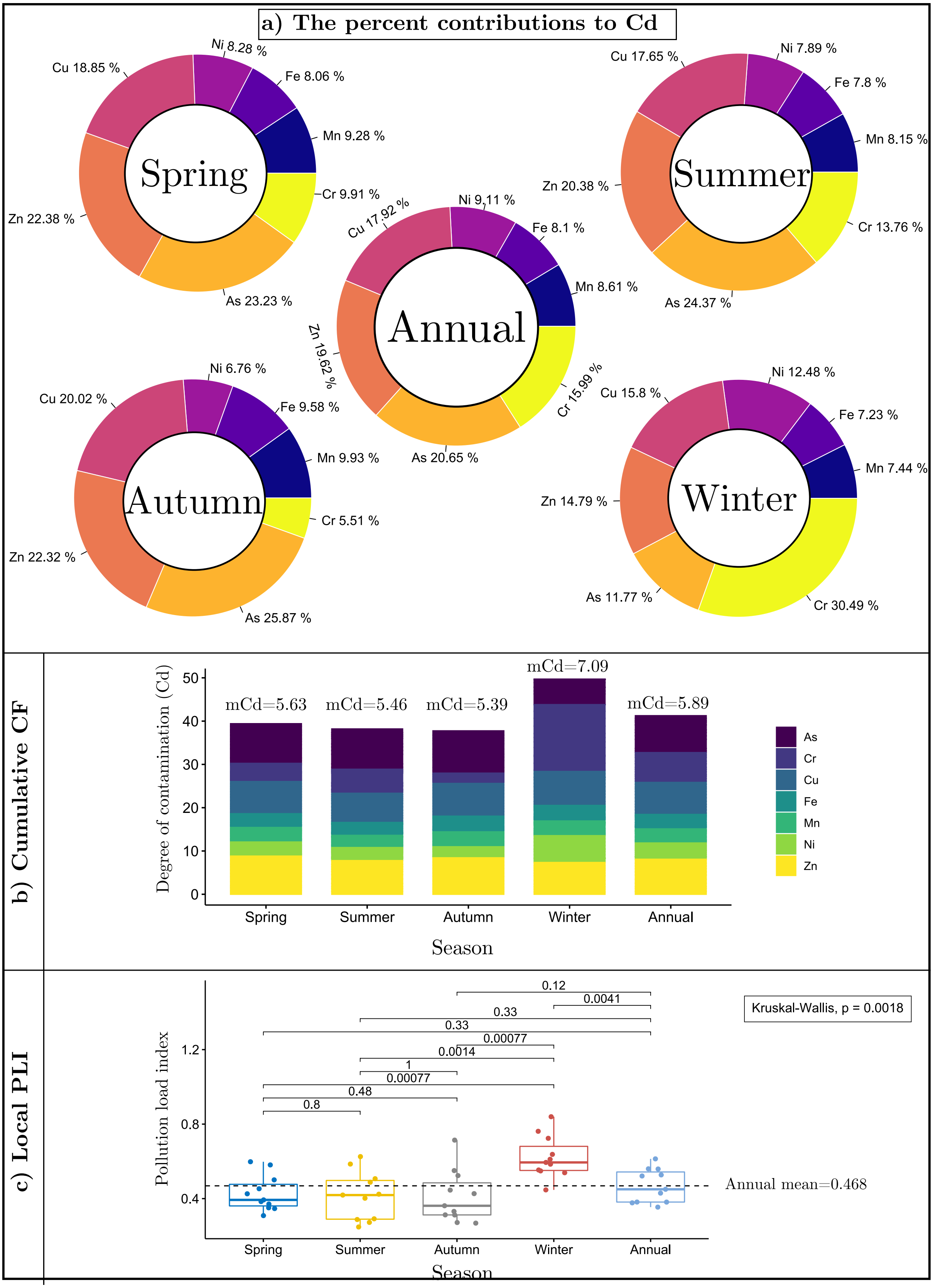

Fig. 4 Diagrams showing the seasonal distribution of contamination factors (CF), contamination degree (Cd), and Pollution Load Index (PLI) levels

The average E_r values for the metals were ranked as follows: As (8.97), Cu (3.44), Ni (1.88), Cr (1.20), Zn (0.74), Mn (0.33), and Fe (0.30). Since all E_r values were below 15, there is no significant ecological risk due to the toxicity of the metals in the studied area. Figure 5 illustrates the seasonal contributions of the metals to the *PERI*. In all seasons, As was the primary contributor to the ecological risk, while Fe contributed the least. These findings align with the pollution levels observed in Fig. 5a. Additionally, seasonal variations in *PERI* are shown in Fig. 5b, where winter had the highest *PERI* due to increased Cr contamination. The mean *PERI* for the study area was 15.4, with the highest value in winter (15.8) and the lowest in summer (15.1). These values indicate that the region has a very low ecological risk (*PERI* < 50) (Table S3) (Gopal et al. 2021, 2023). The Mann–Whitney test found no significant seasonal differences in *PERI* values ($p > 0.05$), suggesting that metal pollution is relatively stable across different seasons. However, localized risk areas should still be monitored due to the potential for accumulation in marine organisms (Yalçın et al. 2023).

Potential human health risk assessment

Non-carcinogenic risk and carcinogenic risk

The *ADI*, *HQ*, *HI*, *CR*, and *TCR* values are shown in Table 3. The following is a ranking of the ADI_{total} distribution for metals in sediments in the study region: Zn > Cr > Cu > Ni > As > Fe > Mn. These findings indicate that Zn has the highest potential for exposure, whereas Mn has the lowest, which is consistent with previous studies on coastal metal contamination in Turkey and India (Baltas et al. 2020; Gopal et al. 2021).Adults had the highest ADI_{total} values for oral intake, consistent with other research results (Chabukdhara and Nema 2013; Wei et al. 2015; Eziz et al. 2018; Baltas et al. 2020).

The PTE *HQ* values were graded as follows: As > Cr > Fe > Ni > Mn > Cu > Zn. The *HQs* for adults ranged from 5.39E − 04 to 5.24E − 02. This suggests that the primary exposure pathway for PTEs in the study area is oral consumption, which aligns with findings from Mediterranean and Southeast Asian coastal risk assessments (Chabukdhara and Nema 2013; Wei et al. 2015; Eziz et al. 2018). The *HI* value for adults was 0.131, which is below the safety threshold (*HI* < 1). This confirms that non-carcinogenic risks from PTEs in the study area are currently insignificant, consistent with previous marine sediment studies (Wu et al. 2020).

The *CR* and *TCR* values for the carcinogenic metals (Cr, Ni, and As) are summarized in Table 3. The calculated total carcinogenic risk (CR_{total}) values ranged from 3.10E − 05 to 4.64E − 05, with Cr having the highest carcinogenic risk. This suggests that Cr poses a more significant long-term health risk than Ni and As, consistent with previous reports on Cr-related carcinogenic risks in marine ecosystems (Eziz et al. 2018; Wu et al. 2020). The *TCR* for adults was found to be 1.21E − 04, which falls within the acceptable cancer risk range (10^{-6}–10^{-4}). These results indicate a low but non-negligible carcinogenic risk, aligning with studies from the Caspian Sea and Red Sea, where Cr was the dominant carcinogenic element (Nour et al. 2019; El-Sorogy et al. 2020).

A comparison of carcinogenic (*CR)* and non-carcinogenic (*HI*) health risks according to exposure pathways and seasonal fluctuations is shown in Fig. 6. *HI* values for ingestion (Fig. 6a) did not show significant seasonal differences (Kruskal–Wallis test, $p > 0.05$), except for winter ($p < 0.05$). The Mann–Whitney pairwise comparison confirmed that winter exhibited the highest ingestion-related *HI* risk, likely due to increased runoff and industrial discharges (Gopal et al. 2023). *HI* values for dermal exposure (Fig. 6b) also showed no significant variations across seasons ($p > 0.05$). Figure 6b shows the seasonal variations in the *HI* dermal route. When the seasonal averages were considered, both the Kruskal–Wallis and the Mann–Whitney pairwise comparison tests revealed no significant difference between the *HI* levels resulting from the dermal pathway ($p > 0.05$).

The *CR* ingestion pathway (Fig. 6c) showed significant seasonal variation ($p < 0.05$), with winter having the highest *CR* values. Mann–Whitney tests indicated that the winter season significantly differed from other seasons ($p < 0.05$). This is in line with previous studies indicating that Cr and As contamination peaks during rainy seasons due to increased runoff from anthropogenic sources (Öztürk et al. 2021). The dermal route *CR* levels (Fig. 6d) also varied significantly ($p < 0.05$), particularly in autumn, when mean dermal-derived *CR* values differed from annual mean levels and the means of other seasons.

The spatial distribution of potentially toxic element contents in sediments

Figure 7 displays the seasonal spatial horizontal distribution contour maps of the PTEs. It can be observed that, in spring, all PTEs except As and Cr exhibit similar behavior. As for arsenic (As), high concentrations were observed between stations 3 and 4, while high convcentrations of Cr were found between stations 8 and 10. When evaluating Fig. 7 for summer, attention is drawn to the similar distribution patterns between Fe, Ni, and Zn, as well as between Mn and Cu. Additionally, the highest concentration of As was measured at station 2, while the lowest levels were found between stations 8 and 10. High levels of Cr were detected only around the 7th and 8th stations, with low concentrations found at all other stations. When evaluating Fig. 7, a similar distribution pattern during autumn is observed among Mn and the elements Fe, Cu, Ni, and Zn. Furthermore, it was found that the concentration of As followed a comparable distribution

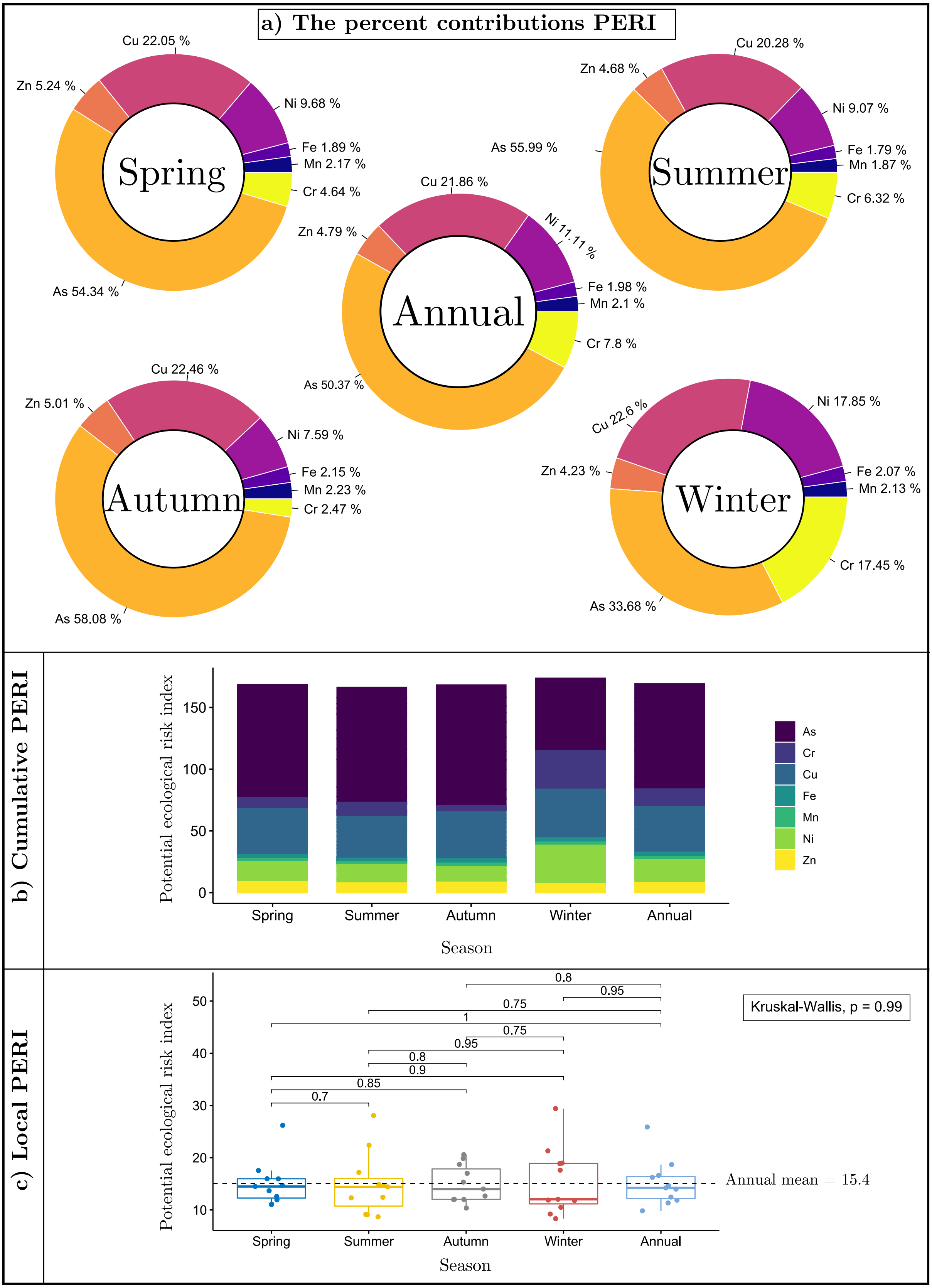

Fig. 5 For potential ecological risk levels (PERI) from potentially toxic elements, seasonal contribution of elements and cumulative PERI values

Table 3 Description of the health risk indexes in sediment

Elements	ADI_{ing}	ADI_{derm}	ADI_{total}
Cr	9.02E – 05	3.42E – 07	9.06E – 05
Mn	4.01E – 04	1.6E – 06	4.03E – 04
Fe	2.04E – 02	8.14E – 05	2.05E – 02
Ni	4.29E – 05	1.71E – 07	4.31E – 05
Cu	4.91E – 05	1.96E – 07	4.93E – 05
Zn	9.46E – 05	3.77E – 07	9.50E – 05
As	1.67E – 05	1.97E – 06	1.86E – 05
Elements	CR_{ing}	CR_{derm}	CR_{total}
Cr	4.51E – 05	6.84E – 06	5.20 E – 05
Mn			
Fe			
Ni	3.91E – 05	7.28E – 06	4.64 E – 05
Cu			
Zn			
As	2.50E – 05	5.98E – 06	3.10 E – 05
Elements	HQ_{ing}	HQ_{derm}	HQ_{total}
Cr	3.01E – 02	5.59E – 03	4.73E – 02
Mn	2.87E – 03	3.73E – 03	7.79E – 03
Fe	2.91E – 02	6.61E – 04	2.36E – 02
Ni	2.15E – 03	1.77E – 04	9.48E – 03
Cu	1.23E – 03	2.54E – 05	1.37E – 03
Zn	3.15E – 04	8.31E – 06	5.39E – 04
As	5.55E – 02	1.14E – 02	5.24E – 02

TCR		
Min	Max	Mean
4.77E – 05	2.83E – 04	1.21E – 04

HI		
Min	Max	Mean
6.23E – 02	2.79E – 01	1.31E – 01

to the distrubition during summer, with the highest levels observed around station 3 and the lowest levels between stations 8 and 10. Additionally, the significant fluctuations in the distribution of Cr between the 6th and 10th stations are noteworthy. Finally, when evaluating Fig. 7 for winter, it is noteworthy that the distribution patterns of Fe and Zn are similar to those observed during summer. Additionally, while the lowest levels of Mn and Cu are found at the same station (9th station), the stations where the highest levels are observed differ (6th station for Mn, and stations 1 through 5 for Cu). It is observed that Fe, Ni, and Zn exhibit a similar distribution structure. Although Ni was detected at low levels between the 2nd and 3rd stations, it was not found to be evenly distributed throughout the study area. The distribution of As was similar to that observed in autumn, with the highest levels observed around the 3rd station and the lowest levels between the 8th and 10th stations. In this season, the study area had a high concentration of Cr, and the lowest concentration was found at station 3. Regarding the element As, it was also present in the study area, but its distribution was not specified. These spatial trends align with previous sediment mapping studies, where Cr and As contamination hotspots were linked to anthropogenic activities (Yalçın et al. 2023; Akçay 2024).

Figure 8 displays the comparative seasonal distribution maps of environmental pollution levels (*PLI*) and ecological risk levels (*PERI*). The *PLI* levels were generally low at the 1st and 2nd stations in spring, autumn, and winter, while the lowest levels were observed around the 10th station in summer. The highest *PLI* levels were observed between the 5th and 6th stations in summer, autumn, and winter, and between the 4th and 5th stations in spring. The distribution

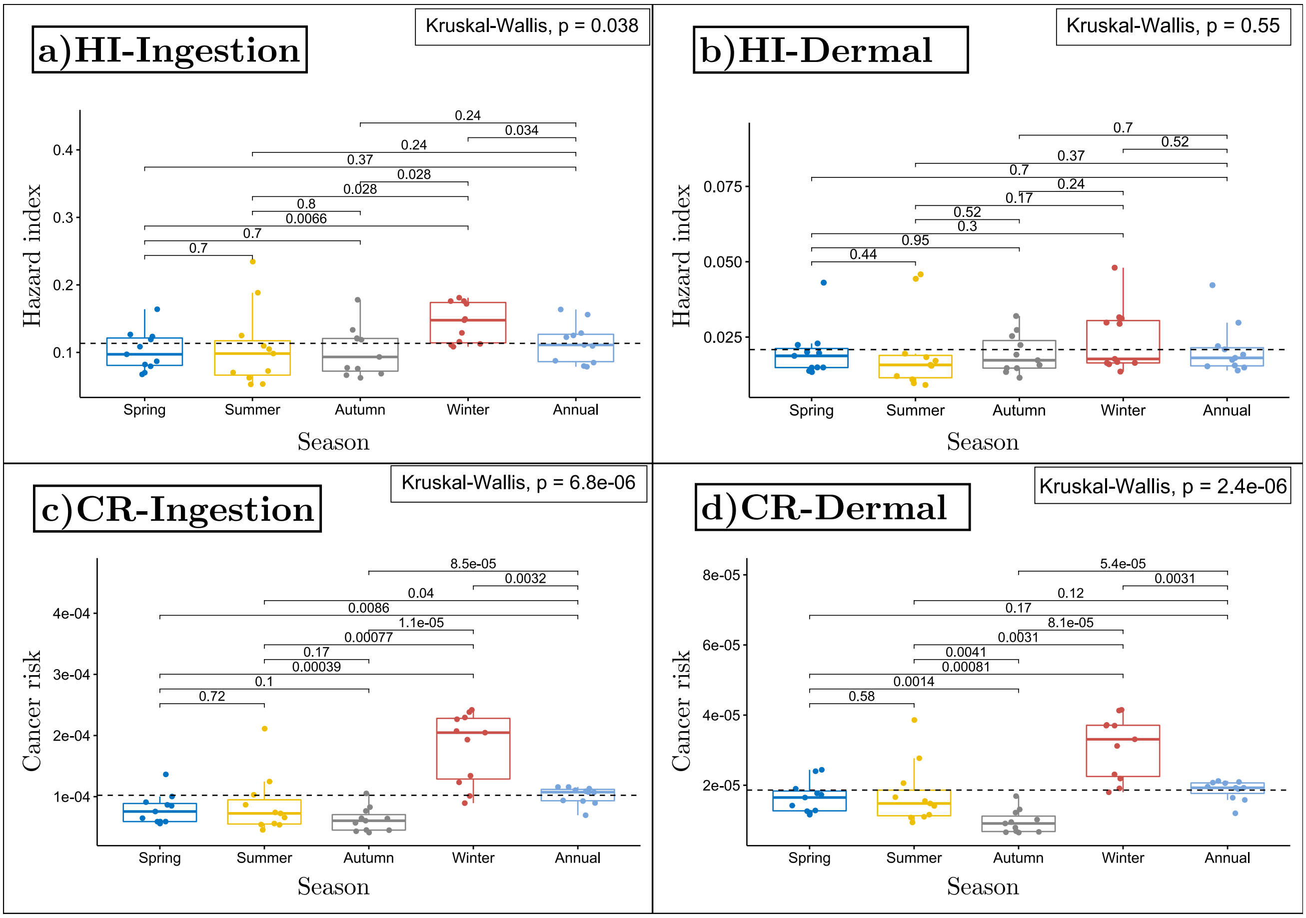

Fig. 6 Seasonal variations of carcinogenic (CR) and non-carcinogenic (HI) health risks and overall comparison by exposure pathways

patterns of *PERI* values were generally similar across seasons. The lowest *PERI* levels were observed between the 8th and 10th stations, while the highest levels were observed between the 3rd and 4th stations in each season.

Figure 9 displays comparative distribution maps of carcinogenic (*CR*) and non-carcinogenic (*HI*) health risks based on seasonal variations, and routes of exposure (ingestion and dermal). The hazard index (*HI*) levels exhibit similar distribution patterns in each season for both ingestion and dermal routes. Station 3 consistently exhibits the highest *HI* levels across all seasons, while station 6 shows a significant increase in summer, autumn, and winter compared to its levels in other seasons. The lowest *HI* levels are consistently observed at stations 9 and 10, and stations 1, and 2, across all seasons. When analyzing cancer risk (*CR*) levels, both ingestion and dermal routes, had a similar distribution structure in all seasons except winter. The highest levels were detected around station 4 and station 8 in winter, around station 6 in autumn and summer, and around station 9 in spring. In spring, the lowest *CR* levels were detected around the 1st and 2nd stations. In summer, they were detected between the 9th and 10th stations. In autumn, they were detected both at the 1st and 2nd stations and between the 9th and 10th stations. In winter, the lowest *CR* levels were detected around the third station for ingestion and the second station for dermal exposure.

Multivariate analysis of potentially toxic elements in sediments

The Pearson correlation coefficients among the concentrations of PTEs in the sediment are shown in Fig. S1. The correlation analysis reveals that PTE contamination in Alanya's coastal sediments is driven by both geogenic and anthropogenic influences. A strong correlation is observed between Mn and Fe ($r = 0.79$), suggesting their origin from natural weathering and sediment transport, which is consistent with studies in Giresun, Türkiye where these elements were linked to lithogenic sources (Yalçın et al. 2023). Similarly, the strong correlation between Zn and Fe ($r = 0.80$) suggests that Zn has both natural and anthropogenic sources, aligning with research in Çandarlı Gulf, where Fe, Zn, and Cu were associated with industrial and agricultural runoff (Duman et al. 2025). The correlation between Cu and Zn ($r = 0.66$)

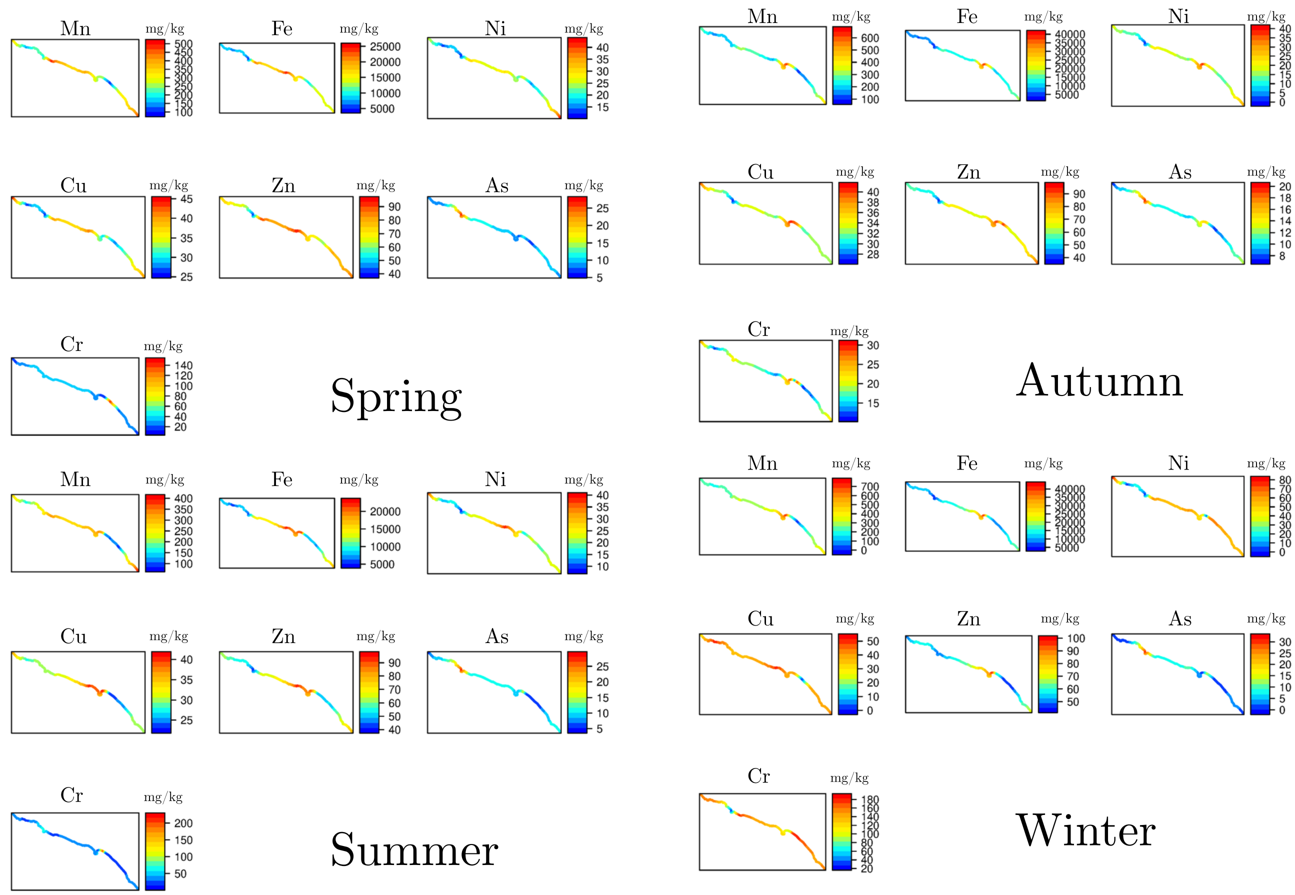

Fig. 7 Spatial distribution maps of elements according to seasons

suggests their connection to fertilizer and pesticide residues, a pattern also observed in Akyatan Lagoon, Türkiye where agricultural runoff was identified as a primary pollution source (Özbay et al. 2025). Additionally, Ni and Cr ($r = 0.46$) show a moderate correlation, which may indicate urbanization and tourism-related pollution, like findings from Al-Uqair, Saudi Arabia, where these metals were linked to vehicular emissions and coastal development (Abbasi et al. 2020). The weak or negative correlations observed for As with other metals suggest that As originates from distinct sources, likely related to pesticide application, as supported by studies in the Mediterranean coastal region (Atakoglu et al. 2024).

The relationships between PTEs in sediments and their potential sources were examined using Principal Component Analysis (PCA). The Kaiser–Meyer–Olkin (KMO) measure was 0.66, indicating that the dataset was suitable for PCA (Ji et al. 2019; Liu et al. 2023). The Bartlett's sphericity test ($p < 0.05$) confirmed that the variables were significantly correlated, making PCA an effective tool for source determination (Baltas et al. 2020; Apaydın et al. 2022). Two major components with eigenvalues greater than 1 explained 69.951% of the total variance in the dataset (Table 4). Fig. S2 visually represents the relationships between PTEs, with PC1 and PC2 distinguishing between natural and anthropogenic sources (Öztürk et al. 2021). According to Liu et al. (2003) and Ustaoğlu and Islam (2020), factor loadings were classified as weak (0.30–0.50), moderate (0.50–0.75), or strong (> 0.75).

The first principal component (PC1, which accounts for 50.234% of the total variance) exhibited strong positive loadings for Mn, Fe, and Zn, while Cu and Ni showed moderate positive loadings (Table 4). The dominance of Fe and Mn in PC1 suggests natural sources such as geogenic inputs, rock weathering, and coastal erosion (Zhu et al. 2013; Liu et al. 2023). However, Zn and Cu displayed enrichment factors (EF) > 1.5, indicating that they are influenced by anthropogenic activities such as vehicle emissions, industrial waste, and aquaculture (Sun et al. 2019; Zhang et al. 2020). Additionally, fertilizer and pesticide applications in agricultural areas are potential contributors to Cu and Zn levels, particularly in regions where

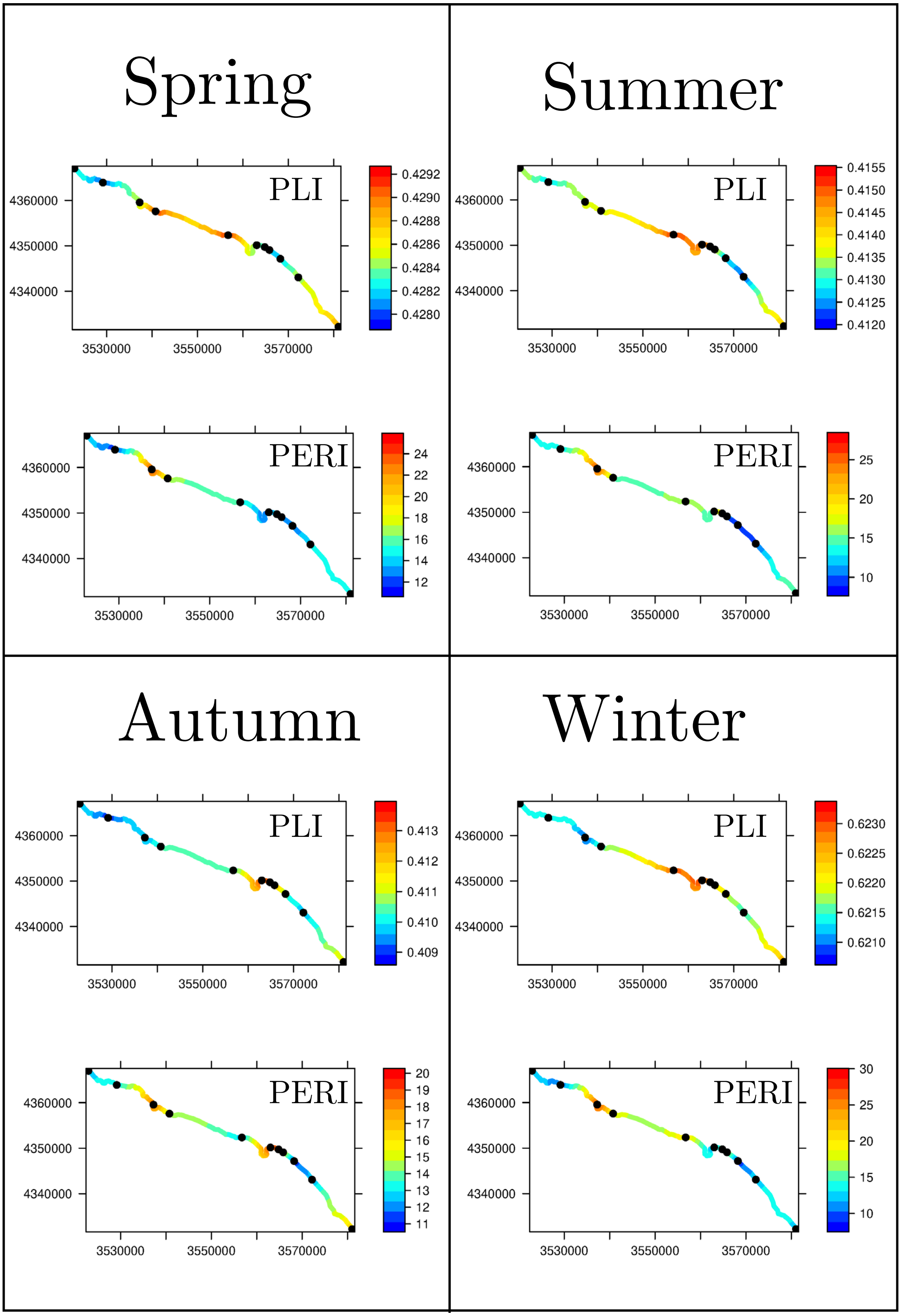

Fig. 8 Comparison of seasonal distribution maps of pollution load index (PLI) and potential ecological risk levels (PERI) levels

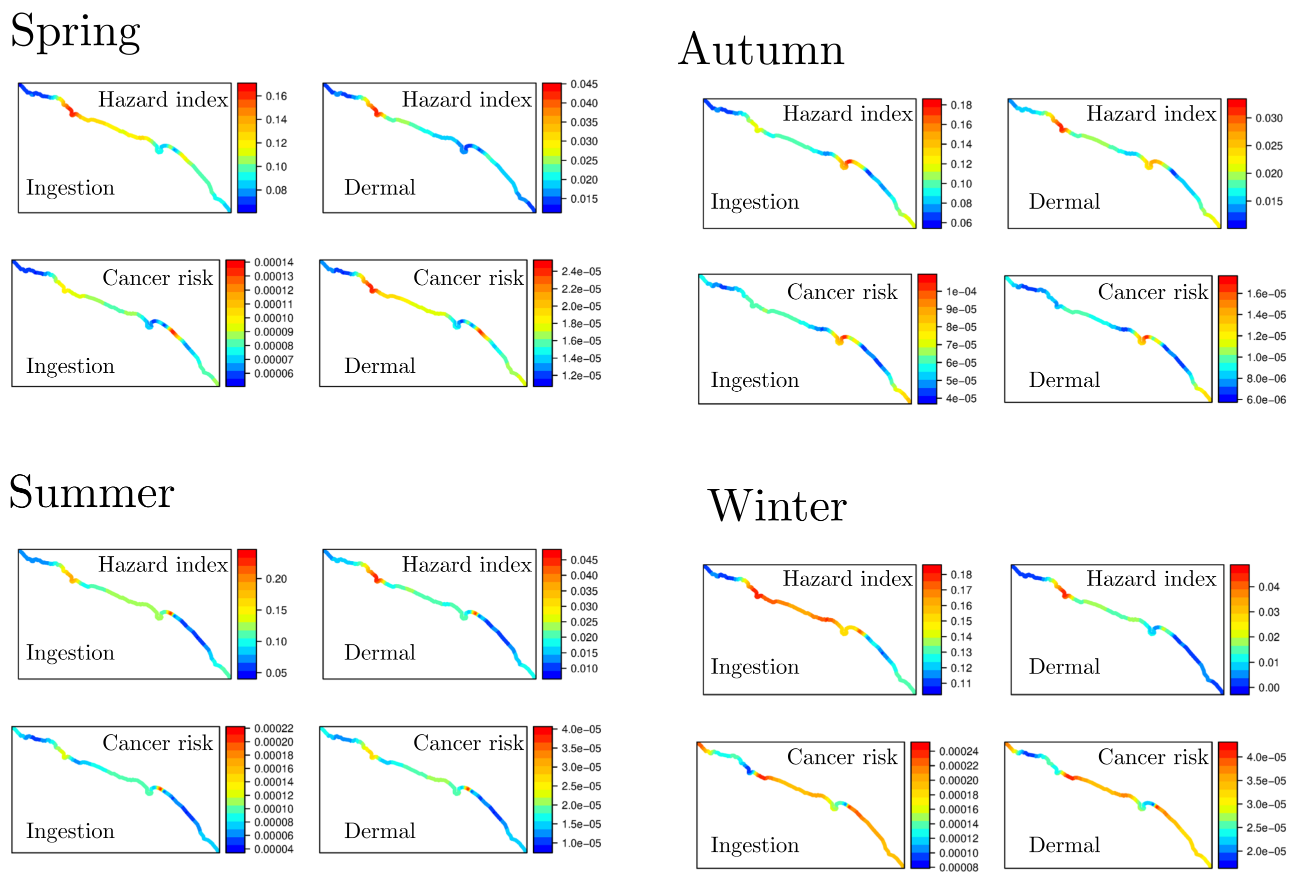

Fig. 9 Comparison of seasonal distribution maps of cancer risk (carcinogenic, CR) and Hazard index (non-carcinogenic, HI) health risks according to seasonal distribution and routes of exposure (ingestion and dermal)

Table 4 Rotated component matrix of metals in sediments

Parameter	PC1	PC2
Mn	**0.834**	0.381
Fe	**0.874**	0.136
Ni	**0.738**	0.053
Cu	**0.831**	0.084
Zn	**0.907**	−0.175
Cr	0.055	**0.838**
As	0.058	**0.684**
Eigenvalues	**3.622**	**1.274**
% of variance	**50.234**	**19.627**
Cumulative %	**50.234**	**69.951**

Values in bold indicate loadings above a threshold (0.5), considered relevant for interpretation

bananas, citrus fruits, and kiwis are cultivated (Chen et al. 2018; Song et al. 2019). The increasing presence of Zn and Cu in coastal sediments may also be linked to tourism-related pollution and coastal boat traffic (Ustaoğlu and Islam 2020).

In contrast, Mn and Ni exhibited *EF* values lower than 1.5, indicating that their primary sources are natural processes such as rock weathering and sediment transport (Savitha et al. 2018). Mn, which is commonly derived from silicate mineral weathering, follows a similar distribution pattern to that reported in Black Sea and Mediterranean coastal sediments (Yalçın et al. 2023). These findings suggest that PC1 represents a combination of geogenic and anthropogenic sources, including riverine input, industrial processes, aquaculture, and urbanization (Kelepertzis 2014; Chandrasekaran and Ravisankar 2015; Ma et al. 2016; Baltas et al. 2017).

The second principal component (PC2, explaining 19.627% of the variance) exhibited a strong positive loading for Cr and a moderate positive loading for As. The *EF* values for Cr and As were found to be greater than 1.5, confirming that these elements originate primarily from anthropogenic sources such as industrial discharge, vehicle emissions, and agricultural runoff (Çevik et al. 2008; Baltas et al. 2017; Liu et al. 2023). Cr contamination is commonly associated with industrial waste, untreated sewage, and electroplating, while As contamination often originates from pesticide use, mining activities, and coal combustion (Sun et al. 2019; Ben-Tahar et al. 2025). The seasonal variation in Cr and As concentrations further supports the idea that their input is influenced by rainfall-induced runoff and urban wastewater discharges, similar to findings from previous studies in Mediterranean and Indian coastal zones (Gopal et al. 2018, 2023).

The PCA results from this study align with those of previous research. In the Eastern Black Sea, Cr and As were identified as dominant anthropogenic pollutants, supporting the classification of PC2 in this study (Yalçın et al. 2023). Research on Red Sea sediments found that Mn and Fe primarily originated from natural sources, consistent with the PC1 findings (Nour et al. 2019; El-Sorogy et al. 2020). A study in Turkish coastal areas also identified Zn and Cu as contaminants linked to industrial and urban wastewater; this matches the PC1 findings of this study (Apaydın et al. 2022). Similarly, a study on the Southeast Indian shelf found that industrial effluents significantly contributed to Cr and As contamination, supporting the observed influence of PC2 (Gopal et al. 2021).

These results highlight the need for targeted pollution control strategies focusing on metals with significant anthropogenic influence (Cr, As, Cu, Zn). While Fe, Mn, and Ni primarily originate from natural sources, their accumulation in marine environments should still be monitored over time to assess potential long-term impacts. In contrast, Cr, As, Cu, and Zn pollution suggests direct human impacts, necessitating better wastewater treatment, stricter emission controls, and improved environmental regulations (Baltas et al. 2017; Gopal et al. 2019). Long-term monitoring should also be conducted to assess seasonal trends in metal pollution and develop effective mitigation strategies for high-risk periods, particularly in winter and the rainy seasons, when runoff-driven contamination peaks (Gopal et al. 2019).

Hierarchical cluster analysis (HCA) identified three main PTE clusters, confirming multiple contamination sources in Alanya (Fig. S3). Fe, Mn, and Zn form a cluster, indicating a dominant lithogenic origin, consistent with findings from the Pearl River Estuary, where Fe and Mn are linked to weathering and hydrodynamic forces (Liang et al. 2025). Cu and Zn cluster together, suggesting mixed sources; Cu is primarily influenced by agricultural runoff and wastewater discharge, this trend is observed in Cuddalore, India (Vinothkannan et al. 2022). Cr, Ni, and As form a separate group, pointing to industrial discharges and historical pesticide contamination, similar to Mediterranean sediment studies (Atakoglu et al. 2024). These results highlight the need for improved wastewater treatment and better management of agricultural runoffs to mitigate sediment contamination.

Conclusions

This study analyzed the concentrations, distribution, and potential risks of potentially toxic elements (PTEs) in sediment samples, revealing significant variability among metals. The findings indicated that Fe was the most abundant metal, followed by Mn, Zn, Cr, Cu, Ni, and As. The Kolmogorov–Smirnov (K–S) test, along with skewness and kurtosis values, confirmed that the metal concentrations followed a normal distribution. Moreover, the coefficient of variation (CV) values suggested that Cr showed the highest variability, due to anthropogenic influences, while Cu exhibited minimal fluctuations, likely indicating a natural origin.

The enrichment factor (*EF*), geo-accumulation index (I_{geo}), contamination factor (C_f), modified degree of contamination (mC_d), and pollution load index (*PLI*) were employed to assess pollution. While *EF* values indicated moderate enrichment for Cu, Zn, Cr, and As, and minimal enrichment for Ni and Mn, the I_{geo} results classified the sediments as unpolluted. Additionally, the contamination factor values showed minimal contamination, and the *PLI* values confirmed that the area remained unpolluted overall.

The ecological risk factor (E_r) and the potential ecological risk (*PERI*) assessments indicated a very low ecological risk for all metals, with As being the primary contributor. Similarly, human health risk assessments revealed that the non-carcinogenic risk (*HI*) values were below the threshold, indicating no significant health hazard. However, the carcinogenic risk (*CR*) analysis showed that Cr posed the highest risk among the studied elements, although overall cancer risk remained within the low-risk category.

Overall, the study area is not significantly polluted, and the ecological and human health risks posed by PTEs remain low. However, continuous monitoring is essential to track potential anthropogenic influences and prevent future contamination. Further studies should focus on identifying specific pollution sources and implementing effective management strategies to maintain environmental and public health safety.

Supplementary Information The online version contains supplementary material available at https://doi.org/10.1007/s12665-025-12263-8.

Acknowledgements This work was supported by the Coordinator of Scientific Research Projects of Alanya Alaaddin Keykubat University with the project number 2021-02-08-MAP06.

Author contributions Erhan Cengiz, Murat Şirin, and Gökhan Apaydın: Conceptualization, Methodology and Software. Murat Şirin, and Erhan Cengiz: Data curation and Writing- Original draft preparation. Cafer Mert Yeşilkanat, and Murat Şirin: Visualization and investigation. Erhan Cengiz: Supervision. Erhan Cengiz, and Gökhan Apaydın: Validation. Murat Şirin, and Erhan Cengiz: Writing- Reviewing and Editing.

Funding Open access funding provided by the Scientific and Technological Research Council of Türkiye (TÜBİTAK).

Data availability No datasets were generated or analysed during the current study.

Declarations

Conflict of interest The authors declare no competing interests.

Ethics approval Not applicable.

Consent to participate Not applicable.

Consent to publish Not applicable.

References

Abbasi A, Mirekhtiary F (2020) Heavy metals and natural radioactivity concentration in sediments of the Mediterranean Sea coast. Mar Pollut Bull 154:111041. https://doi.org/10.1016/j.marpolbul.2020.111041

Abdelaal A, Lasheen ESR, Mansour AM et al (2024) Assessing the ecological and health risks associated with heavy metal pollution levels in sediments of Big Giftun and Abu Minqar Islands, East Hurghada, Red Sea, Egypt. Mar Pollut Bull 198:115930. https://doi.org/10.1016/j.marpolbul.2023.115930

Adimalla N (2020) Heavy metals contamination in urban surface soils of Medak province, India, and its risk assessment and spatial distribution. Environ Geochem Health 42:59–75. https://doi.org/10.1007/s10653-019-00270-1

Akçay İ (2024) Environmental risk assessment and bioaccumulation of heavy metals in sediments and macroalgae (Enteromorpha sp) along the Mersin Coast (Türkiye), Northeastern Mediterranean Sea. Reg Stud Mar Sci 77:103673. https://doi.org/10.1016/j.rsma.2024.103673

Alkan N, Alkan A, Demirak A, Bahloul M (2020) Metals/metalloid in marine sediments, bioaccumulating in macroalgae and a mussel. Soil Sediment Contam Int J 29:569–594. https://doi.org/10.1080/15320383.2020.1751061

Anandkumar A, Nagarajan R, Prabakaran K, Rajaram R (2017) Trace metal dynamics and risk assessment in the commercially important marine shrimp species collected from the Miri coast, Sarawak, East Malaysia. Reg Stud Mar Sci 16:79–88. https://doi.org/10.1016/j.rsma.2017.08.007

Anandkumar A, Nagarajan R, Prabakaran K et al (2018) Human health risk assessment and bioaccumulation of trace metals in fish species collected from the Miri coast, Sarawak, Borneo. Mar Pollut Bull 133:655–663. https://doi.org/10.1016/j.marpolbul.2018.06.033

Apaydın A, Kabaoğlu H, Apaydın G et al (2022) Evaluation of ecological risk, source, and spatial distribution of some heavy metals in marine sediments in the Middle and Eastern Black Sea region, Turkey. Environ Sci Pollut Res 29:7053–7066. https://doi.org/10.1007/s11356-021-16017-4

Atakoglu OO, Berberoglu E, Yalcin F et al (2024) Source identification of heavy metal contamination in beach sediments of the ancient city of Phaselis in Antalya, Türkiye. Int J Sedim Res 39:942–959. https://doi.org/10.1016/j.ijsrc.2024.09.003

Aydın H, Tepe Y, Ustaoğlu F (2023) A holistic approach to the eco-geochemical risk assessment of trace elements in the estuarine sediments of the Southeastern Black Sea. Mar Pollut Bull 189:114732. https://doi.org/10.1016/j.marpolbul.2023.114732

Bai J, Cui B, Chen B et al (2011) Spatial distribution and ecological risk assessment of heavy metals in surface sediments from a typical plateau lake wetland, China. Ecol Modell 222:301–306. https://doi.org/10.1016/j.ecolmodel.2009.12.002

Balaram V, Subramanyam KSV (2022) Sample preparation for geochemical analysis: Strategies and significance. Adv Sample Prep 1:100010. https://doi.org/10.1016/j.sampre.2022.100010

Baltas H, Sirin M, Dalgic G et al (2017) Assessment of metal concentrations (Cu, Zn, and Pb) in seawater, sediment and biota samples in the coastal area of Eastern Black Sea, Turkey. Mar Pollut Bull 122:475–482. https://doi.org/10.1016/j.marpolbul.2017.06.059

Baltas H, Yesilkanat CM, Kiris E, Sirin M (2019) A study of the radiological baseline conditions around the planned Sinop (Turkey) nuclear power plant using the mapping method. Environ Monit Assess 191:660. https://doi.org/10.1007/s10661-019-7819-z

Baltas H, Sirin M, Gökbayrak E, Ozcelik AE (2020) A case study on pollution and a human health risk assessment of heavy metals in agricultural soils around Sinop province, Turkey. Chemosphere 241:125015. https://doi.org/10.1016/j.chemosphere.2019.125015

Bastami KD, Neyestani MR, Shemirani F et al (2015) Heavy metal pollution assessment in relation to sediment properties in the coastal sediments of the southern Caspian Sea. Mar Pollut Bull 92:237–243. https://doi.org/10.1016/j.marpolbul.2014.12.035

Bell AMT, Backhouse DJ, Deng W et al (2020) X-ray fluorescence analysis of feldspars and silicate glass: effects of melting time on fused bead consistency and volatilisation. Minerals 10:442. https://doi.org/10.3390/min10050442

Ben-Tahar R, Basraoui NE, Boukich O et al (2025) Potentially toxic elements contamination and health risk assessment of coastal sediments in Betoya Bay, Morocco. Environ Monit Assess 197:19. https://doi.org/10.1007/s10661-024-13495-0

Böke Özkoç H, Arıman S (2023) Contamination and risk assessment of heavy metals in coastal sediments from the Mid-Black Sea, Turkey. Stoch Env Res Risk Assess 37:375–394. https://doi.org/10.1007/s00477-022-02300-4

Bonsignore M, Manta DS, Sharif EAA-T et al (2018) Marine pollution in the Libyan coastal area: environmental and risk assessment. Mar Pollut Bull 128:340–352. https://doi.org/10.1016/j.marpolbul.2018.01.043

Boukich O, Ben-Tahar R, Basraoui NE et al (2024) Assessment of heavy metal pollution and related risks to human health a case of Angads plain, Morocco. J Ecol Eng 25:354–366. https://doi.org/10.12911/22998993/191438

Cai L, Xu Z, Bao P et al (2015) Multivariate and geostatistical analyses of the spatial distribution and source of arsenic and heavy metals in the agricultural soils in Shunde, Southeast China. J Geochem Explor 148:189–195. https://doi.org/10.1016/j.gexplo.2014.09.010

Cai L-M, Wang Q-S, Wen H-H et al (2019) Heavy metals in agricultural soils from a typical township in Guangdong Province, China: occurrences and spatial distribution. Ecotoxicol Environ Saf 168:184–191

Çevik U, Damla N, Kobya AI et al (2008) Assessment of metal element concentrations in mussel (*M. galloprovincialis*) in Eastern Black Sea, Turkey. J Hazard Mater 160:396–401. https://doi.org/10.1016/j.jhazmat.2008.03.010

Chabukdhara M, Nema AK (2013) Heavy metals assessment in urban soil around industrial clusters in Ghaziabad, India: probabilistic health risk approach. Ecotoxicol Environ Saf 87:57–64. https://doi.org/10.1016/j.ecoenv.2012.08.032

Chandrasekaran A, Ravisankar R (2015) Spatial distribution of physico-chemical properties and function of heavy metals in soils of Yelagiri hills, Tamilnadu by energy dispersive X-ray florescence spectroscopy (EDXRF) with statistical approach. Spectrochim Acta A Mol Biomol Spectrosc 150:586–601. https://doi.org/10.1016/j.saa.2015.05.083

Chen L, Zhou S, Wu S et al (2018) Combining emission inventory and isotope ratio analyses for quantitative source apportionment of heavy metals in agricultural soil. Chemosphere 204:140–147. https://doi.org/10.1016/j.chemosphere.2018.04.002

Croffie MET, Williams PN, Fenton O et al (2020) Optimising sample preparation and calibrations in EDXRF for quantitative soil analysis. Agronomy 10:1309. https://doi.org/10.3390/agronomy10091309

Cui X, Wang X, Liu B (2020) The characteristics of heavy metal pollution in surface dust in Tangshan, a heavily industrialized city in North China, and an assessment of associated health risks. J Geochem Explor 210:106432. https://doi.org/10.1016/j.gexplo.2019.106432

Custodio M, Espinoza C, Orellana E et al (2022) Assessment of toxic metal contamination, distribution and risk in the sediments from lagoons used for fish farming in the central region of Peru. Toxicol Rep 9:1603–1613. https://doi.org/10.1016/j.toxrep.2022.07.016

Damek-Poprawa M, Sawicka-Kapusta K (2003) Damage to the liver, kidney, and testis with reference to burden of heavy metals in yellow-necked mice from areas around steelworks and zinc smelters in Poland. Toxicology 186:1–10. https://doi.org/10.1016/S0300-483X(02)00595-4

Du Laing G, Rinklebe J, Vandecasteele B et al (2009) Trace metal behaviour in estuarine and riverine floodplain soils and sediments: a review. Sci Total Environ 407:3972–3985. https://doi.org/10.1016/j.scitotenv.2008.07.025

Duman M, Eronat AH, Talas E et al (2025) Understanding heavy Metal pollution dynamics in Çandarlı Gulf, western Türkiye: Insights from spatial analysis, sediment transport modeling and ecological risk assessment. Cont Shelf Res 285:105393. https://doi.org/10.1016/j.csr.2024.105393

Edokpayi JN, Odiyo JO, Popoola EO, Msagati TAM (2017) Evaluation of temporary seasonal variation of heavy metals and their potential ecological risk in Nzhelele River, South Africa. Open Chem 15:272–282. https://doi.org/10.1515/chem-2017-0033

El Nemr A, El-Said GF (2017) Assessment and ecological risk of heavy metals in sediment and molluscs from the Mediterranean coast. Water Environ Res 89:195–210. https://doi.org/10.2175/106143016X14798353399458

El-Said GF, Draz SEO, El-Sadaawy MM, Moneer AA (2014) Sedimentology, geochemistry, pollution status and ecological risk assessment of some heavy metals in surficial sediments of an Egyptian lagoon connecting to the Mediterranean Sea. J Environ Sci Health, Part A 49:1029–1044. https://doi.org/10.1080/10934529.2014.894853

El-Sorogy AS, Youssef M, Al-Kahtany K, Saleh MM (2020) Distribution, source, contamination, and ecological risk status of heavy metals in the Red Sea-Gulf of Aqaba coastal sediments, Saudi Arabia. Mar Pollut Bull 158:111411. https://doi.org/10.1016/j.marpolbul.2020.111411

Eziz M, Mohammad A, Mamut A, Hini G (2018) A human health risk assessment of heavy metals in agricultural soils of Yanqi Basin, Silk Road Economic Belt, China. Hum Ecol Risk Assess Int J 24:1352–1366. https://doi.org/10.1080/10807039.2017.1412818

Ferreira-Baptista L, De Miguel E (2005) Geochemistry and risk assessment of street dust in Luanda, Angola: a tropical urban environment. Atmos Environ 39:4501–4512. https://doi.org/10.1016/j.atmosenv.2005.03.026

Field A, Miles J, Field Z (2012) Discovering Statistics Using R. SAGE Publications Ltd., California, USA (**ISBN: 9781446200469**)

Ge J, Woodward LA, Li QX, Wang J (2013) Composition, distribution and risk assessment of organochlorine pesticides in soils from the Midway Atoll, North Pacific Ocean. Sci Total Environ 452–453:421–426. https://doi.org/10.1016/j.scitotenv.2013.03.015

Gholizadeh M, Patimar R (2018) Ecological risk assessment of heavy metals in surface sediments from the Gorgan Bay, Caspian Sea. Mar Pollut Bull 137:662–667. https://doi.org/10.1016/j.marpolbul.2018.11.009

Gopal V, Nithya B, Magesh NS, Jayaprakash M (2018) Seasonal variations and environmental risk assessment of trace elements in the sediments of Uppanar River estuary, southern India. Mar Pollut Bull 129:347–356. https://doi.org/10.1016/j.marpolbul.2018.03.003

Gopal V, Krishnamurthy RR, Chakraborty P et al (2019) Trace element contamination in marine sediments along the southeast Indian shelf following Cyclone Gaja. Mar Pollut Bull 149:110520. https://doi.org/10.1016/j.marpolbul.2019.110520

Gopal V, Krishnamurthy RR, Kiran DRS et al (2020) Trace metal contamination in the marine sediments off Point Calimere, Southeast coast of India. Mar Pollut Bull 161:111764. https://doi.org/10.1016/j.marpolbul.2020.111764

Gopal V, Krishnamurthy RR, Sreeshma T et al (2021) Effect of a tropical cyclone on the distribution of heavy metals in the marine sediments off Kameswaram, Southeast coast of India. Mar Pollut Bull 171:112741. https://doi.org/10.1016/j.marpolbul.2021.112741

Gopal V, Krishnamurthy RR, Vignesh R et al (2023) Assessment of heavy metal contamination in the surface sediments of the Vedaranyam coast, Southern India. Reg Stud Mar Sci 65:103081. https://doi.org/10.1016/j.rsma.2023.103081

Gope M, Masto RE, George J et al (2017) Bioavailability and health risk of some potentially toxic elements (Cd, Cu, Pb and Zn) in street dust of Asansol, India. Ecotoxicol Environ Saf 138:231–241. https://doi.org/10.1016/j.ecoenv.2017.01.008

Gu Y-G, Lin Q, Huang H-H et al (2017) Heavy metals in fish tissues/stomach contents in four marine wild commercially valuable fish species from the western continental shelf of South China Sea. Mar Pollut Bull 114:1125–1129. https://doi.org/10.1016/j.marpolbul.2016.10.040

Gui D, Yu R-Q, Karczmarski L et al (2017) Spatiotemporal trends of heavy metals in Indo-Pacific humpback dolphins (Sousa chinensis) from the western Pearl River Estuary, China. Environ Sci Technol 51:1848–1858. https://doi.org/10.1021/acs.est.6b05566

Gülşen-Rothmund Hİ, Arslan Ş, Kurtuluş B et al (2023) Assessment of trace metal pollution in the coastal sediments of Fethiye-Göcek Bay (SW Turkey) and evaluation of pollution sources. Mar Pollut Bull 186:114387. https://doi.org/10.1016/j.marpolbul.2022.114387

Hogstrand C, Haux C (1991) Binding and detoxification of heavy metals in lower vertebrates with reference to metallothionein. Comp Biochem Physiol Part c: Comp Pharmacol 100:137–141. https://doi.org/10.1016/0742-8413(91)90140-O

Hossain MM, Hannan ASMA, Kamal MM et al (2022) Appraisal and validation of a method used for detecting heavy metals in poultry feed in Bangladesh. Vet World 15:2217. https://doi.org/10.14202/vetworld.2022.2217-2223

Islam MS, Uddin MK, Tareq SM et al (2015) Alteration of water pollution level with the seasonal changes in mean daily discharge in three main rivers around Dhaka City, Bangladesh. Environments 2:280–294. https://doi.org/10.3390/environments2030280

Jain CK, Gupta H, Chakrapani GJ (2008) Enrichment and fractionation of heavy metals in bed sediments of River Narmada, India. Environ Monit Assess 141:35–47. https://doi.org/10.1007/s10661-007-9876-y

Jayarathne A, Egodawatta P, Ayoko GA, Goonetilleke A (2018) Assessment of ecological and human health risks of metals in urban road dust based on geochemical fractionation and potential bioavailability. Sci Total Environ 635:1609–1619. https://doi.org/10.1016/j.scitotenv.2018.04.098

Ji Z, Zhang Y, Zhang H et al (2019) Fraction spatial distributions and ecological risk assessment of heavy metals in the sediments of Baiyangdian Lake. Ecotoxicol Environ Saf 174:417–428. https://doi.org/10.1016/j.ecoenv.2019.02.062

Kadachi AN, Al-Eshaikh MA (2012) Limits of detection in XRF spectroscopy. X-Ray Spectrom 41:350–355. https://doi.org/10.1002/xrs.2412

Kamunda C, Mathuthu M, Madhuku M (2016) Health risk assessment of heavy metals in soils from Witwatersrand Gold Mining Basin, South Africa. Int J Environ Res Public Health 13:663. https://doi.org/10.3390/ijerph13070663

Ke X, Gui S, Huang H et al (2017) Ecological risk assessment and source identification for heavy metals in surface sediment from the Liaohe River protected area, China. Chemosphere 175:473–481. https://doi.org/10.1016/j.chemosphere.2017.02.029

Kelepertzis E (2014) Accumulation of heavy metals in agricultural soils of Mediterranean: insights from Argolida basin, Peloponnese, Greece. Geoderma 221–222:82–90. https://doi.org/10.1016/j.geoderma.2014.01.007

Khalil MK, Draz SEO, El Zokm GM, El-Said GF (2016) Apportionment of geochemistry, texture's properties, and risk assessment of some elements in surface sediments from Bardawil Lagoon, Egypt. Hum Ecol Risk Assess: Int J 22:775–791. https://doi.org/10.1080/10807039.2015.1107714

Kırıs E, Baltas H (2021) Assessing pollution levels and health effects of heavy metals in sediments around Cayeli copper mine area, Rize, Turkey. Environ Forensics 22:372–384. https://doi.org/10.1080/15275922.2020.1850572

Kodat M, Tepe Y (2023) A holistic approach to the assessment of heavy metal levels and associated risks in the coastal sediment of Giresun, southeast Black Sea. Heliyon 9:e16424. https://doi.org/10.1016/j.heliyon.2023.e16424

Krauskopf KB (1985) Introduction to geochemistry, 1st edn. Mc Grow-Hill book company (**ISBN 007–y 66382–66383**)

Kumar SB, Padhi RK, Mohanty AK, Satpathy KK (2017) Elemental distribution and trace metal contamination in the surface sediment of southeast coast of India. Mar Pollut Bull 114:1164–1170. https://doi.org/10.1016/j.marpolbul.2016.10.038

Li S, Jia Z (2018) Heavy metals in soils from a representative rapidly developing megacity (SW China): levels, source identification and apportionment. Catena (Amst) 163:414–423. https://doi.org/10.1016/j.catena.2017.12.035.10.1016/j.catena.2017.12.035

Li H-H, Chen L-J, Yu L et al (2017) Pollution characteristics and risk assessment of human exposure to oral bioaccessibility of heavy metals via urban street dusts from different functional areas in Chengdu, China. Sci Total Environ 586:1076–1084. https://doi.org/10.1016/j.scitotenv.2017.02.092

Liang H, Wang G, Guo H et al (2025) Evaluation of heavy metal accumulation and sources in surface sediments of the Pearl River Estuary (China). Mar Environ Res 204:106948. https://doi.org/10.1016/j.marenvres.2025.106948

Ling SY, Junaidi A, Mohd-Harun A et al (2023) Heavy metal pollution assessment in marine sediments in the Northwest coast of Sabah, Malaysia. China Geoly 6:580–593. https://doi.org/10.31035/cg2022079

Liu C-W, Lin K-H, Kuo Y-M (2003) Application of factor analysis in the assessment of groundwater quality in a blackfoot disease area in Taiwan. Sci Total Environ 313:77–89. https://doi.org/10.1016/S0048-9697(02)00683-6

Liu H, Xiong Z, Jiang X et al (2016) Heavy metal concentrations in riparian soils along the Han River, China: the importance of soil properties, topography and upland land use. Ecol Eng 97:545–552. https://doi.org/10.1016/j.ecoleng.2016.10.060

Liu Q, Jia Z, Li S, Hu J (2019) Assessment of heavy metal pollution, distribution and quantitative source apportionment in surface sediments along a partially mixed estuary (Modaomen, China). Chemosphere 225:829–838. https://doi.org/10.1016/j.chemosphere.2019.03.063

Liu X, Sheng Y, Liu Q, Li Z (2023) Ecological and environmental risks of heavy metals in sediments in Dingzi Bay, South Yellow Sea. Mar Pollut Bull 188:114683. https://doi.org/10.1016/j.marpolbul.2023.114683

Liu X, Ding C, Qin H et al (2024) Pollution characteristics, distribution and risk level of heavy metals in sediments of the Yangtze River estuary. Heliyon 10:e28796. https://doi.org/10.1016/j.heliyon.2024.e28796

Long ER, MacDonald DD, Smith SL, Calder FD (1995) Incidence of adverse biological effects within ranges of chemical concentrations in marine and estuarine sediments. Environ Manag 19:81–97. https://doi.org/10.1007/BF02472006

Lu X, Wang L, Li LY et al (2010) Multivariate statistical analysis of heavy metals in street dust of Baoji, NW China. J Hazard Mater 173:744–749. https://doi.org/10.1016/j.jhazmat.2009.09.001

Ma X, Zuo H, Tian M et al (2016) Assessment of heavy metals contamination in sediments from three adjacent regions of the Yellow River using metal chemical fractions and multivariate analysis techniques. Chemosphere 144:264–272. https://doi.org/10.1016/j.chemosphere.2015.08.026

Mamut A, Eziz M, Mohammad A, Anayit M (2017) The spatial distribution, contamination, and ecological risk assessment of heavy metals of farmland soils in Karashahar-Baghrash oasis, northwest China. Hum Ecol Risk Assess 23:1300–1314. https://doi.org/10.1080/10807039.2017.1305263

Marcinkonis S, Baltrenaite E, Lazauskas S (2011) Extraction and mapping of soil factors using factor analysis and geostatistical analysis on intensively manured heterogenous soils. Pol J Environ Stud 20:701–708

Mille T, Cresson P, Chouvelon T et al (2018) Trace metal concentrations in the muscle of seven marine species: comparison between the Gulf of Lions (North-West Mediterranean Sea) and the Bay of Biscay (North-East Atlantic Ocean). Mar Pollut Bull 135:9–16. https://doi.org/10.1016/j.marpolbul.2018.05.051

Ni M, Mao R, Jia Z et al (2018) Heavy metals in soils of Hechuan County in the upper Yangtze (SW China): comparative pollution assessment using multiple indices with high-spatial-resolution sampling. Ecotoxicol Environ Saf 148:644–651. https://doi.org/10.1016/j.ecoenv.2017.11.009

Nour HE, El-Sorogy AS, Abd El-Wahab M et al (2019) Contamination and ecological risk assessment of heavy metals pollution from the Shalateen coastal sediments, Red Sea, Egypt. Mar Pollut Bull 144:167–172. https://doi.org/10.1016/j.marpolbul.2019.04.056

Nour HE, Helal SA, Wahab MA (2022) Contamination and health risk assessment of heavy metals in beach sediments of Red Sea and

Gulf of Aqaba, Egypt. Mar Pollut Bull 177:113517. https://doi.org/10.1016/j.marpolbul.2022.113517
Odabas T, Hajiyev R, Gultekin A et al (2021) Can we prevent coffee stains on teeth? J Med Food 24:1331–1339. https://doi.org/10.1089/jmf.2020.0205
Odediran ET, Adeniran JA, Yusuf RO et al (2021) Contamination levels, health risks and source apportionment of potentially toxic elements in road dusts of a densely populated African City. Environ Nanotechnol Monit Manag 15:100445. https://doi.org/10.1016/j.enmm.2021.100445
Özbay Ö, Akçay İ, Alp MT, Börekçi NS (2025) Distribution of heavy metals in surface sediments of a Coastal Lagoon (Akyatan Lagoon, Northeastern Mediterranean Sea): ecological and potential health risk assessment. Reg Stud Mar Sci 82:104058. https://doi.org/10.1016/j.rsma.2025.104058
Özşeker K, Dürrani Ö, Atasaral Ş, Seyhan K (2025) Assessment of toxic metal contamination in coastal sediments of major fishing ports in the Southeastern Black Sea, Türkiye: spatial distribution, risk evaluation, and source identification. Reg Stud Mar Sci 81:103957. https://doi.org/10.1016/j.rsma.2024.103957
Öztürk RÇ, Gedik K, Şahin A et al (2021) Comparative trace element trends in *Posidonia oceanica* and its sediments along the Turkish-Mediterranean Sea coast. Environ Sci Pollut Res 28:61397–61407. https://doi.org/10.1007/s11356-021-15089-6
Pebesma EJ (2004) Multivariable geostatistics in S: the gstat package. Comput Geosci 30:683–691. https://doi.org/10.1016/J.CAGEO.2004.03.012
Pebesma EJ, Bivand R (2005) Classes and methods for spatial data in R. R News 4:9–13
R Core Team (2024) R: A language and environment for statistical computing. In: R Found. Stat. Comput. http://www.r-project.org/. Accessed 18 Aug 2024
Rajeshkumar S, Liu Y, Zhang X et al (2018) Studies on seasonal pollution of heavy metals in water, sediment, fish and oyster from the Meiliang Bay of Taihu Lake in China. Chemosphere 191:626–638. https://doi.org/10.1016/j.chemosphere.2017.10.078
Ravisankar R, Sivakumar S, Chandrasekaran A et al (2015) Statistical assessment of heavy metal pollution in sediments of east coast of Tamilnadu using energy dispersive X-ray fluorescence spectroscopy (EDXRF). Appl Radiat Isot 102:42–47. https://doi.org/10.1016/j.apradiso.2015.03.018
Sancer O, Tekin-Özan S (2016) Seasonal changes of metal accumulation in water, sediment and *Phragmites austrialis* (Cav.) Trin. ex Steudel Growing in Lake Kovada, Isparta, Türkiye
Savitha S, Srinivasalu S, Suresh S, Jayamoorthy K (2018) Distribution of heavy metals in the marine sediments of various sites in Karaichalli Island, Tuticorin, Gulf of Mannar, India. SILICON 10:1419–1425. https://doi.org/10.1007/s12633-017-9619-9
Şener E, Şener Ş, Bulut C (2023) Assessment of heavy metal pollution and quality in lake water and sediment by various index methods and GIS: a case study in Beyşehir Lake. Turkey Mar Pollut Bull 192:115101. https://doi.org/10.1016/j.marpolbul.2023.115101
Shabbaj II, Alghamdi MA, Shamy M et al (2018) Risk assessment and implication of human exposure to road dust heavy metals in Jeddah, Saudi Arabia. Int J Environ Res Public Health 15:36. https://doi.org/10.3390/ijerph15010036
Soliman NF, Nasr SM, Okbah MA (2015) Potential ecological risk of heavy metals in sediments from the Mediterranean coast, Egypt. J Environ Health Sci Eng 13:1–12. https://doi.org/10.1186/s40201-015-0223-x
Song J, Liu Q, Sheng Y (2019) Distribution and risk assessment of trace metals in riverine surface sediments in gold mining area. Environ Monit Assess 191:1–13. https://doi.org/10.1007/s10661-019-7311-9
Sun C, Zhang Z, Cao H et al (2019) Concentrations, speciation, and ecological risk of heavy metals in the sediment of the Songhua River in an urban area with petrochemical industries. Chemosphere 219:538–545. https://doi.org/10.1016/j.chemosphere.2018.12.040
Tepe Y (2009) Metal concentrations in eight fish species from Aegean and Mediterranean Seas. Environ Monit Assess 159:501–509. https://doi.org/10.1007/s10661-008-0646-2
Tholkappian M, Ravisankar R, Chandrasekaran A et al (2018) Assessing heavy metal toxicity in sediments of Chennai Coast of Tamil Nadu using energy dispersive X-ray fluorescence spectroscopy (EDXRF) with statistical approach. Toxicol Rep 5:173–182. https://doi.org/10.1016/j.toxrep.2017.12.020
Tian K, Huang B, Xing Z, Hu W (2017) Geochemical baseline establishment and ecological risk evaluation of heavy metals in greenhouse soils from Dongtai, China. Ecol Indic 72:510–520. https://doi.org/10.1016/j.ecolind.2016.08.037
USEPA (1989) Risk assessment guidance for superfund human health evaluation manual (Part A). Vol. I. Office of Emergency and Remedial Response. U.S. Environmental Protection Agency, Washington, D.C.
USEPA (1993) Reference dose (RfD): description and use in health risk assessments. Background Document 1A. Integrated risk information system (IRIS). U.S. Environmental Protection Agency, Washington, DC
USEPA (1996) Soil screening guidance: technical background document. EPA/540/r-95/128. Office of Solid Waste and Emergency Response
USEPA (2002) Supplemental guidance for developing soil screening levels for superfund sites. U.S. Environmental Protection Agency, Washington, DC
USEPA (2010) Estimation of Relative Bioavailablity of Lead in Soil and Soil-like Materials Using in Vivo and in Vitro Methods. OSWER 9285.7–77. Solid Waste and Emergency Response, U.S. Environmental Protection Agency, Washington, DC
Ustaoğlu F, Islam MS (2020) Potential toxic elements in sediment of some rivers at Giresun, Northeast Turkey: a preliminary assessment for ecotoxicological status and health risk. Ecol Indic 113:106237. https://doi.org/10.1016/j.ecolind.2020.106237
Ustaoğlu F, Tepe Y (2019) Water quality and sediment contamination assessment of Pazarsuyu Stream, Turkey using multivariate statistical methods and pollution indicators. Int Soil Water Conserv Res 7:47–56. https://doi.org/10.1016/j.iswcr.2018.09.001
Varol M, Sünbül MR (2018) Multiple approaches to assess human health risks from carcinogenic and non-carcinogenic metals via consumption of five fish species from a large reservoir in Turkey. Sci Total Environ 633:684–694. https://doi.org/10.1016/j.scitotenv.2018.03.218
Vinothkannan A, Charles PE, Rajaram R (2022) Ecological risk assessment and seasonal variation of heavy metals in water and sediment collected from industrially polluted Cuddalore coast, Southeastern India. Reg Stud Mar Sci 49:102134. https://doi.org/10.1016/j.rsma.2021.102134
Wang G, Zhang Y, Wang J et al (2021) Spatial distribution and ecological risk assessment of heavy metals in sediments of a heavily polluted Maozhou River, Southern China. Bull Environ Contam Toxicol 106:844–851. https://doi.org/10.1007/s00128-021-03202-x
Wei B, Yang L (2010) A review of heavy metal contaminations in urban soils, urban road dusts and agricultural soils from China. Microchem J 94:99–107. https://doi.org/10.1016/j.microc.2009.09.014
Wei B, Jiang F, Li X, Mu S (2009) Spatial distribution and contamination assessment of heavy metals in urban road dusts from

Urumqi, NW China. Microchem J 93:147–152. https://doi.org/10.1016/j.microc.2009.06.001
Wei X, Gao B, Wang P et al (2015) Pollution characteristics and health risk assessment of heavy metals in street dusts from different functional areas in Beijing, China. Ecotoxicol Environ Saf 112:186–192. https://doi.org/10.1016/j.ecoenv.2014.11.005
Wu H, Yang F, Li H et al (2020) Heavy metal pollution and health risk assessment of agricultural soil near a smelter in an industrial city in China. Int J Environ Health Res 30:174–186. https://doi.org/10.1080/09603123.2019.1584666
Yalçın MG, Mutlu E, Olguner C et al (2023) Spatial geochemical structure of soft sediment on shallow littoral of the Gulf of Antalya, the eastern Mediterranean Sea. Mar Pollut Bull 193:115155. https://doi.org/10.1016/j.marpolbul.2023.115155
Yesilkanat CM, Kobya Y (2021) Spatial characteristics of ecological and health risks of toxic heavy metal pollution from road dust in the Black Sea coast of Turkey. Geoderma Reg 25:e00388. https://doi.org/10.1016/j.geodrs.2021.e00388
Zaqoot HA, Aish AM, Wafi HN (2018) Study on heavy metal pollution in Gaza fishing harbour along the Mediterranean Sea-Gaza beach, Palestine. J Aquat Sci Mar Biol 1:24–34. https://doi.org/10.22259/2638-5481.0101005
Zhang P, Qin C, Hong X et al (2018) Risk assessment and source analysis of soil heavy metal pollution from lower reaches of Yellow River irrigation in China. Sci Total Environ 633:1136–1147. https://doi.org/10.1016/j.scitotenv.2018.03.228
Zhang M, Chen G, Luo Z et al (2020) Spatial distribution, source identification, and risk assessment of heavy metals in seawater and sediments from Meishan Bay, Zhejiang coast, China. Mar Pollut Bull 156:111217. https://doi.org/10.1016/j.marpolbul.2020.111217
Zhao S, Shi X, Li C et al (2014) Seasonal variation of heavy metals in sediment of Lake Ulansuhai, China. Chem Ecol 30:1–14. https://doi.org/10.1080/02757540.2013.841894
Zhao L, Hu G, Yan Y et al (2019) Source apportionment of heavy metals in urban road dust in a continental city of eastern China: using Pb and Sr isotopes combined with multivariate statistical analysis. Atmos Environ 201:201–211. https://doi.org/10.1016/j.atmosenv.2018.12.050
Zhu X, Ji H, Chen Y et al (2013) Assessment and sources of heavy metals in surface sediments of Miyun Reservoir, Beijing. Environ Monit Assess 185:6049–6062. https://doi.org/10.1007/s10661-012-3005-2
Zhuang S, Lu X (2020) Environmental risk evaluation and source identification of heavy metal (loid) s in agricultural soil of Shangdan Valley, Northwest China. Sustainability 12:5806. https://doi.org/10.3390/su12145806